Inorganic Chemistry
Article

Inorg. Chem. **2010**, *49*, 5241–5261 **5241**
DOI: 10.1021/ic100344f

Six-Membered Electron Transfer Series $[V(dithiolene)_3]^z$ ($z = 1+, 0, 1-, 2-, 3-, 4-$). An X-ray Absorption Spectroscopic and Density Functional Theoretical Study

Stephen Sproules,*,† Thomas Weyhermüller,† Serena DeBeer,‡ and Karl Wieghardt*,†

†*Max-Planck-Institut für Bioanorganische Chemie, Stiftstrasse 34-36, D-45470 Mülheim an der Ruhr, Germany, and* ‡*Department of Chemistry and Chemical Biology, Baker Laboratory, Cornell University, Ithaca, New York 14853*

Received February 20, 2010

The electronic structures of vanadium centers coordinated by three dithiolene ligands have been elucidated by using a host of physical methods: X-ray crystallography, cyclic voltammetry, electronic absorption, electron paramagnetic resonance (EPR), and X-ray absorption spectroscopies, augmented by density functional theoretical (DFT) calculations. The consensus electronic structure derived from this approach is a V(IV) central ion for the neutral, monoanionic, and dianionic members of this electron transfer series, where the tris(dithiolene) ligand units are $(L_3)^{4-}$, $(L_3)^{5-\bullet}$, and $(L_3)^{6-}$, respectively. The trigonal prismatic monoanions, $[V^{IV}(L_3^{5-\bullet})]^{1-}$ (S=0), are defined as singlet diradicals where the crystallographically observed dithiolene fold results from strong antiferromagnetic coupling between the metal- and ligand-based magnetic orbitals. These results are contrasted with the corresponding tris(dioxolene)vanadium electron transfer series toward establishing the factors that govern the molecular trigonal prismatic or octahedral geometries in systems with three redox noninnocent ligands.

Introduction

The neutral tris(dithiolene)vanadium complexes $[V(pdt)_3]^0$ and $[V(edt)_3]^0$ have been independently synthesized and characterized by elemental analyses and spectroscopy (infrared, UV−vis, and electron paramagnetic resonance (EPR)) by the groups of Schrauzer et al.,[1−3] Holm et al.,[4] and Gray et al.[5,6] in 1965/1966 ($(pdt)^{2-}$ represents *cis*-1,2-diphenylethene-1,2-dithiolate(2−) and $(edt)^{2-}$ is 1,2-ethylenedithiolate(2−) as shown in Scheme 2). In 1966 the crystal structure of $[V(pdt)_3]^0$ was determined by film techniques at room temperature by Eisenberg, Stiefel, Rosenberg, and Gray.[5,6] The structure of $[V(edt)_3]^0$ reported in 1996 was also determined at 295 K though using an automated four-circle diffractometer.[7] In both cases a trigonal prismatic VS_6 coordination polyhedron has been established. As summarized in Table 1, a third structure of such a neutral complex, namely, $[V(dddt)_3]^0$, where $(dddt)^{2-}$ represents 5,6-dihydro-1,4-dithiine-2,3-dithiolate(2−),[8] has been reported where the trigonal prismatic VS_6 polyhedron is somewhat distorted with a twist angle Θ of 15.7° ($\Theta = 0°$ for a regular trigonal prism and 60° for an octahedron, Scheme 1).

Electrochemically, it has been established[4,6,9,10] that these and other tris(dithiolene)vanadium complexes (neutral and negatively charged species) constitute an electron transfer series where the neutral forms can be reversibly transformed by one-electron transfer waves to the corresponding mono-, di-, and trianions: $[V(L)_3]^z$ ($z = 0, 1-, 2-, 3-$). In the case of the series $[V(mnt)_3]^{1-,2-,3-}$ ($(mnt)^{2-}$ = maleonitriledithiolate) a tetraanion is also electrochemically accessible, whereas the corresponding neutral species was not accessible within the potential window.

Interestingly, $[V(pdt)_3]^0$ may be electrochemically one-electron oxidized to the monocation $[V(pdt)_3]^{1+}$ which is very unstable in solution, but a tetraanion has not been detected in this series.

*To whom correspondence should be addressed. E-mail: sproules@mpi-muelheim.mpg.de (S.S.), wieghardt@mpi-muelheim.mpg.de (K.W.).

(1) Schrauzer, G. N.; Finck, H. W.; Mayweg, V. P. *Angew. Chem.* **1964**, *76*, 715.
(2) Schrauzer, G. N.; Mayweg, V. P. *J. Am. Chem. Soc.* **1966**, *88*, 3235.
(3) Waters, J. H.; Williams, R.; Gray, H. B.; Schrauzer, G. N.; Finck, H. W. *J. Am. Chem. Soc.* **1964**, *86*, 4198.
(4) Davison, A.; Edelstein, N.; Holm, R. H.; Maki, A. H. *Inorg. Chem.* **1965**, *4*, 55.
(5) Eisenberg, R.; Gray, H. B. *Inorg. Chem.* **1967**, *6*, 1844.
(6) Eisenberg, R.; Stiefel, E. I.; Rosenberg, R. C.; Gray, H. B. *J. Am. Chem. Soc.* **1966**, *88*, 2874.
(7) Kondo, M.; Minakoshi, S.; Iwata, K.; Shimizu, T.; Matsuzaka, H.; Kamigata, N.; Kitagawa, S. *Chem. Lett.* **1996**, 489.
(8) Livage, C.; Fourmigué, M.; Batail, P.; Canadell, E.; Coulon, C. *Bull. Soc. Chim. Fr.* **1993**, *130*, 761.
(9) McCleverty, J. A.; Locke, J.; Wharton, E. J.; Gerloch, M. *J. Chem. Soc. A* **1968**, 816.
(10) Wharton, E. J.; McCleverty, J. A. *J. Chem. Soc. A* **1969**, 2258.
(11) Best, S. P.; Ciniawsky, S. A.; Humphrey, D. G. *J. Chem. Soc., Dalton Trans.* **1996**, 2945.

Published on Web 05/03/2010

Table 1. X-ray Crystallographically Characterized [V(dithiolene)$_3$]^z Species[a]

complex	avg. Θ[b]	geometry	avg. α[b]	ref.
Neutral Complexes ($S = {}^1/_2$)				
$[V(pdt)_3]^0$ (1a)	4.9°	t.p.	2.5°	this work 5, 6
$[V(edt)_3]^0$	1.6°	t.p.	0.9°	7
$[V(dddt)_3]^{0c}$	15.7°	t.p.	0.5°	8
Monoanionic Complexes ($S = 0$)				
$[NEt_4][V(pdt)_3]$ (1b)	0.8°	t.p.	23.7°	this work
$[PPh_4]$ $[V(bdt)_3]$ (3b)	1.3°	t.p.	22.6°	this work
$[NBu_4][V(dddt)_3]$	1.8°	t.p.	22.5°	12
$[TTF][V(dddt)_3]$ [d]	5.9°	t.p.	23.4°	8
$[NEt_4][V(bddt)_3]$ [e]	7.2°	t.p.	22.9°	13
$[BEDT]_3[V(dmit)_3]_2$ [f]	4.6°	t.p.	24.8°	14
Dianionic Complexes ($S = {}^1/_2$)				
$[PPh_4]_2[V(mnt)_3]$ (2c)	38.0°	dist. oct.	4.3°	this work
$[AsPh_4]_2[V(mnt)_3]$		dist. oct.		15
$[NMe_4]_2[V(mnt)_3]$		dist. oct.		16
$[TTF]_2[V(mnt)_3]$	39.7°	dist. oct.	24.0°	17
$[NEt_4]_2[V(bdt)_3]$	37.3°	dist. oct.	12.3°	7
$[NEt_4]_2[V(tdt)_3]$	38.9°	dist. oct.	9.3°	7
$[NEt_4]_2[V(dmcdt)_3]$ [g]	34.3°	dist. oct.	3.3°	18
$[NMP]_2[V(dmit)_3]$ [h]	38.2°	dist. oct.	12.0°	19
$[NBu_4]_2[V(dmit)_3]$				20
$[PPh_4]_2[V(dbddto)_3]$ [i]	40.6°	dist. oct.	11.1°	21

[a] Abbreviations: t.p. = trigonal prismatic; oct. = octahedral; dist. = distorted. [b] Defined in Scheme 1. [c] $(dddt)^{2-}$ = 5,6-dihydro-1,4-dithiine-2,3-dithiolate. [d] TTF^+ = tetrathiafulvalenium. [e] $(bddt)^{2-}$ = 1,4-butanediyldithioethylene-1,2-dithiolate. [f] $BEDT^+$ = bis(ethylenedithio)tetrathiafulvalenium, dmit = 2-thioxo-1,3-dithiole-4,5-dithiolate. [g] $(dmcdt)^{2-}$ = dimethylcarboxyethylenedithiolate. [h] NMP = *N*-methylphenazinium. [i] $(dbddto)^{2-}$ = 2,5-dithioxobenzo[1,2-*d*:3,4-*d*′]bis[1,3]dithiolene-7,8-dithiolate.

Solid materials of salts containing mono- and dianions have been prepared and characterized (Table 1). Structurally, two different salts containing the diamagnetic monoanion $[V(dddt)_3]^{1-}$ have been characterized.[8,12] The VS_6 coordination polyhedron is trigonal prismatic irrespective of the nature of the cation $[TTF]^+$ or $[NEt_4]^+$, as well as for $[V(bddt)_3]^{1-}$ (Θ = 7.2°) containing the highly flexible 1,4-butanediyldithioethylene-1,2-dithiolate ligand.[13] Here we report for the first time the structures of $[NEt_4][V(pdt)_3]\cdot 2CH_2Cl_2$ (**1b**) and $[PPh_4][V(bdt)_3]$ (**3b**) where the monoanions are also trigonal prismatic.

Different salts containing paramagnetic dianions $[V(L)_3]^{2-}$ ($S = {}^1/_2$) have been synthesized and structurally characterized (Table 1).[7,8,14−24] Here we report the structure of the salt

Scheme 1. (a) Twist Angle, Θ, Defined As the Dihedral Angle between the Two Essentially Coplanar S_3 Planes of a MS_6 Polyhedron, and (b) Chelate Fold Angles, α, α′, α″, Defined As the Dihedral Angle between the MS_2 and S_2C_2 Planes along the S···S Vector

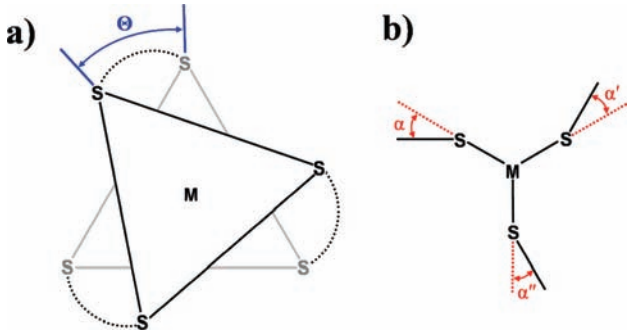

$[PPh_4]_2[V(mnt)_3]\cdot 2CH_2Cl_2$ (**2c**). Three other salts containing the dianion $[V(mnt)_3]^{2-}$ have been structurally characterized previously.[15−17,22−24] The VS_6 polyhedron is (distorted) octahedral (Θ ∼ 39°) irrespective of the nature of the cation.

The electronic structures of the neutral tris(dithiolene)-vanadium species and their reduced mono- and dianions have been discussed controversially in the past because the degree of oxidation of the three dithiolene ligands, $3(L)^{2-}$, in all of these complexes, had not been experimentally established. The neutral complex was the best evidence for ligand oxidation since coordination of three closed-shell dianionic ligands, $(L_3)^{6-}$, would imply a V(VI) oxidation state![3] Therefore, a degree of ligand oxidation must exist through stepwise one-, two-, or three-electron oxidation yielding the $(L_3)^{5-\bullet}$, $(L_3)^{4-}$, or $(L_3)^{3-\bullet}$ units, respectively. These ligand-centered oxidations would yield S-centered π radicals (delocalized) or a diamagnetic $(L_3)^{4-}$ unit. The ambiguity in assigning oxidation levels of the central metal ion and the three ligands remains the main issue in this electron transfer series.

All neutral tris(dithiolene)vanadium species possess an $S = {}^1/_2$ ground state with one unpaired electron; the question then is whether the electron is metal-centered[5,15] generating a $[V^{IV}(L_3{}^{4-})]$ species where $(L_3)^{4-}$ is diamagnetic and the V(IV) ion paramagnetic (d^1, $S = {}^1/_2$) or, alternatively, whether there is a $[V^V(L_3{}^{5-\bullet})]^0$ species present with a paramagnetic $(L_3)^{5-\bullet}$ unit ($S_L = {}^1/_2$) and a diamagnetic V(V) ion (d^0, $S = 0$).[4,23] Another conceivable structure is $[V^{III}(L_3{}^{3-})]^0$ that also gives rise to a ligand-centered unpaired electron. The X-band EPR spectra of all neutral species are very similar displaying the characteristic eight-line pattern of vanadium ($I = {}^7/_2$, 100% natural abundance) with isotropic g and A values at ∼1.99 and ∼60×10^{-4} cm^{-1}, respectively (for a compilation of the data see Table 7 in reference 12) and Table 3 in this work.

Eisenberg and Gray[5] have described the present consensus electronic structure of **1a** in the following fashion: In a trigonal prismatic structure of **1a** the ground state is described as $(4e')^4(3a_1')^1 = {}^2A_1$ where the $(4e')^4$ levels are assigned to the diamagnetic ligand unit $(L_3)^{4-}$ which in turn indicates the presence of two oxidation holes in the closed shell $(L_3)^{6-}$ unit and the $(3a_1')^1$ SOMO corresponds to a $(d_{z^2})^1$ vanadium orbital. This interpretation as $[V^{IV}(L_3{}^{4-})]^0$ is solely based on the analysis of the solution EPR spectrum which was later confirmed by single crystal EPR spectroscopy by Kwik and Stiefel.[15]

The distorted octahedral dianions $[V(L)_3]^{2-}$ also possess an $S = {}^1/_2$ ground state.[15,22] Their EPR spectra are virtually

(12) Welch, J. H.; Bereman, R. D.; Singh, P. *Inorg. Chem.* **1988**, *27*, 2862.
(13) Chung, G.; Bereman, R.; Singh, P. *J. Coord. Chem.* **1994**, *33*, 331.
(14) Broderick, W. E.; McGhee, E. M.; Godfrey, M. R.; Hoffman, B. M.; Ibers, J. A. *Inorg. Chem.* **1989**, *28*, 2902.
(15) Kwik, W.-L.; Stiefel, E. I. *Inorg. Chem.* **1973**, *12*, 2337.
(16) Stiefel, E. I.; Dori, Z.; Gray, H. B. *J. Am. Chem. Soc.* **1967**, *89*, 3353.
(17) Matsubayashi, G.-E.; Akiba, K.; Tanaka, T. *Inorg. Chim. Acta* **1989**, *157*, 195.
(18) Mallard, A.; Simonnet-Jégat, C.; Lavanant, H.; Marrot, J.; Sécheresse, F. *Trans. Met. Chem.* **2008**, *33*, 143.
(19) Matsubayashi, G.-E.; Akiba, K.; Tanaka, T. *Inorg. Chem.* **1988**, *27*, 4744.
(20) Olk, R.-M.; Dietzsch, W.; Kirmse, R.; Stach, J.; Hoyer, E.; Golič, L. *Inorg. Chim. Acta* **1987**, *128*, 251.
(21) Okubo, T.; Maeda, R.; Kondo, M.; Kitagawa, S. *Chem. Lett.* **2006**, *35*, 34.
(22) Atherton, N. M.; Winscom, C. J. *Inorg. Chem.* **1973**, *12*, 383.
(23) Davison, A.; Edelstein, N.; Holm, R. H.; Maki, A. H. *J. Am. Chem. Soc.* **1964**, *86*, 2799.
(24) Stiefel, E. I.; Bennett, L. E.; Dori, Z.; Crawford, T. H.; Simo, C.; Gray, H. B. *Inorg. Chem.* **1970**, *9*, 281.

identical with those reported for the neutral species. Thus, the EPR spectrum of $[V(mnt)_3]^{2-}$ displays isotropic g and A values at 1.982 and 58.6 $\times$ 10^{-4} cm^{-1}, respectively.[15] It has been proposed that the $[V(mnt)_3]^{2-}$ dianion possesses the same $^2A_1$ ground state as the neutral complexes.[15] The electronic structure of the dianion is thus best described as $[V^{IV}(L_3^{6-})]^{2-}$ (or $[V^{IV}(L)_3]^{2-}$) containing three closed shell dithiolate(2−) ligands and a central vanadium(IV) ion with a $(d_{z^2})^1$ configuration.

The electronic structure of the diamagnetic monoanions $[V(L)_3]^{1-}$ ($S = 0$) in Table 1 have not been considered in detail in the past which is mainly due to the fact that no spectroscopic data pertaining to this question are available. Since the neutral species and the dianions contain a central V(IV) ion, it appears to be suggestive to propose an electronic structure for these monoanions as $[V^{IV}(L_3^{5-\bullet})]^{1-}$ where $(L_3)^{5-\bullet}$ is a radical ($S_L = {}^1/_2$) with a single oxidative hole distributed over three ligands. The unpaired electron would be coupled antiferromagnetically to the $(d_{z^2})^1$ electron spin at the V(IV) center: $[V^{IV}(L_3^{5-\bullet})]^{1-}$ ($S = 0$).

It is also quite suggestive that further stepwise one-electron reductions of the dianions, $[V^{IV}(L_3^{6-})]^{2-}$, to the tri- and tetraanions are metal-centered processes yielding $[V^{III}(L_3^{6-})]^{3-}$ and $[V^{II}(L_3^{6-})]^{4-}$ ions with $S = 1$ and an $S = {}^3/_2$ ground states, respectively. The monocation $[V(L)_3]^{1+}$ could possess an electronic structure as in $[V^{IV}(L_3^{3-})]^{1+}$ ($S = 0$) or $[V^{V}(L_3^{4-})]^{1+}$ ($S = 0$).

We have now measured the S K-edge X-ray absorption spectra (XAS) of these complexes. This spectroscopic technique has been popularized by the Solomon group[25] and has in recent years been successfully applied to detect π radical character of *S,S*-coordinated dithiolene ligands.[26−34] In addition, we have measured the V K-edge X-ray absorption spectra of the neutral, monoanionic, and dianionic members of this electron transfer series. To calibrate the V K-edge XAS spectra we have also recorded the spectrum of $[V^{III}(dtc)_3]^0$ (**6**) ($S = 1$)[35−37] where $(dtc)^{1-}$ is the redox inert *N,N*-diethyldithiocarbamate ligand. Scheme 2 shows the complexes,

Scheme 2. Ligands and Complexes

Ligands

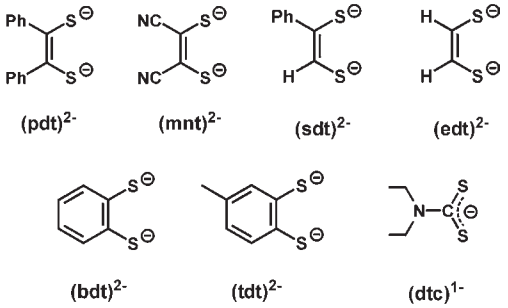

Complexes

$[V(pdt)_3]$	S = 1/2	**1a**
$[NEt_4][V(pdt)_3]$	S = 0	**1b**
$[NEt_4]_2[V(pdt)_3]$	S = 1/2	**1c**
$[PPh_4]_2[V(mnt)_3]$	S = 1/2	**2c**
$[PPh_4][V(bdt)_3]$	S = 0	**3b**
$[PPh_4]_2[V(bdt)_3]$	S = 1/2	**3c**
$[PPh_4][V(tdt)_3]$	S = 0	**4b**
$[PPh_4]_2[V(tdt)_3]$	S = 1/2	**4c**
$[V(edt)_3]$	S = 1/2	**5a**
$[V(dtc)_3]$	S = 1	**6**

ligands, and their abbreviations which are as follows: $[\mathbf{a}]^+$ = monocation, **a** = neutral, **b** = monoanion, **c** = dianion, **d** = trianion, **e** = tetraanion.

The combined approach of metal and ligand K-edge XAS, in concert with EPR measurements, would enable us to experimentally determine the oxidation state of the central vanadium ion (+V d^0; +IV d^1; +III d^2; +II d^3) and the oxidation level of the three dithiolene ligands as $(L_3)^{6-}$ (three equivalent closed-shell dithiolato(2−) ligands), $(L_3)^{5-\bullet}$ ($S_L = {}^1/_2$; one oxidative hole distributed over three ligands), $(L_3)^{4-}$ ($S_L = 0$; two oxidative holes distributed over three ligands), or $(L_3)^{3-}$ ($S_L = {}^3/_2$ or ${}^1/_2$; three oxidative holes distributed over three ligands). Previously, we and others have successfully elucidated the electronic structures for the $[Cr(L)_3]^z$ ($z = 0, 1-, 2-, 3-$),[26,27] $[Re(L)_3]^z$ ($z = 1+, 0, 1-$ $2-$ $3-$)[34] and $[Mo(L)_3]^z$ ($z = 0, 1-$ $2-$)[28,32] electron transfer series.

Finally we have calculated the geometry and electronic structures of the $[V(L)_3]^z$ ($z = 1+, 0, 1-, 2-, 3-, 4-$) series by using density functional theory (DFT) and explored the stability of a trigonal prismatic structure over an octahedral one. In addition, we have used a time-dependent DFT (TD-DFT) protocol to calculate both the vanadium and sulfur K-pre-edge energies as a means to validate the accuracy of the electronic structure description.

Experimental Section

Synthesis of Complexes. All air-sensitive materials were manipulated using standard Schlenk techniques or a glovebox. The ligands benzene-1,2-dithiol, toluene-3,4-dithiol and sodium dithiocarbamate were commercially obtained and used without further purification. The following complexes have been

(25) Glaser, T.; Hedman, B.; Hodgson, K. O.; Solomon, E. I. *Acc. Chem. Res.* **2000**, *33*, 859.
(26) Banerjee, P.; Sproules, S.; Weyhermüller, T.; DeBeer George, S.; Wieghardt, K. *Inorg. Chem.* **2009**, *48*, 5829.
(27) Kapre, R. R.; Bothe, E.; Weyhermüller, T.; DeBeer George, S.; Muresan, N.; Wieghardt, K. *Inorg. Chem.* **2007**, *46*, 7827.
(28) Kapre, R. R.; Bothe, E.; Weyhermüller, T.; DeBeer George, S.; Wieghardt, K. *Inorg. Chem.* **2007**, *46*, 5642.
(29) Pap, J. S.; Benedito, F. L.; Bothe, E.; Bill, E.; DeBeer George, S.; Weyhermüller, T.; Wieghardt, K. *Inorg. Chem.* **2007**, *46*, 4187.
(30) Ray, K.; DeBeer George, S.; Solomon, E. I.; Wieghardt, K.; Neese, F. *Chem.—Eur. J.* **2007**, *13*, 2783.
(31) (a) Sarangi, R.; DeBeer George, S.; Jackson Rudd, D.; Szilagyi, R. K.; Ribas, X.; Rovira, C.; Almeida, M.; Hodgson, K. O.; Hedman, B.; Solomon, E. I. *J. Am. Chem. Soc.* **2007**, *129*, 2316. (b) Szilagyi, R. K.; Lim, B. S.; Glaser, T.; Holm, R. H.; Hedman, B.; Hodgson, K. O.; Solomon, E. I. *J. Am. Chem. Soc.* **2003**, *125*, 9158. (c) Milsmann, C.; Bill, E.; Weyhermüller, T.; DeBeer George, S.; Wieghardt, K. *Inorg. Chem.* **2009**, *48*, 9754.
(32) Tenderholt, A. L.; Szilagyi, R. K.; Holm, R. H.; Hodgson, K. O.; Hedman, B.; Solomon, E. I. *Inorg. Chem.* **2008**, *47*, 6382.
(33) Milsmann, C.; Patra, G. K.; Bill, E.; Weyhermüller, T.; DeBeer George, S.; Wieghardt, K. *Inorg. Chem.* **2009**, *48*, 7430.
(34) Sproules, S.; Benedito, F. L.; Bill, E.; Weyhermüller, T.; DeBeer George, S.; Wieghardt, K. *Inorg. Chem.* **2009**, *48*, 10926.
(35) Bhattacharya, S.; Kanungo, B. K.; Sahoo, S. *J. Coord. Chem.* **2006**, *59*, 371.
(36) Larkworthy, L. F.; O'Donoghue, M. W. *Inorg. Chim. Acta* **1983**, *74*, 155.
(37) Reichel, T. L.; DeHayes, L. J.; Sawyer, D. T. *Inorg. Chem.* **1976**, *15*, 1900.

Table 2. Crystallographic Data for **1a**, **1b**·$2CH_2Cl_2$, **2c**, and **3b**

	1a	**1b**·$2CH_2Cl_2$	**2c**	**3b**
chem. formula	$C_{42}H_{30}S_6V$	$C_{52}H_{54}Cl_4NS_6V$	$C_{60}H_{40}N_6P_2S_6V$	$C_{42}H_{32}PS_6V$
Fw	777.96	1078.06	1150.22	810.95
space group	*C*2/*c*, No. 15	*C*2/*c*, No. 15	*Pbcn*, No. 60	$P2_1/n$, No. 14
a, Å	19.1064(6)	33.385(2)	19.8630(7)	12.8911(12)
b, Å	11.2530(4)	14.5301(7)	15.3255(5)	12.6546(12)
c, Å	17.9293(6)	23.1758(12)	18.0956(6)	22.580(2)
β, deg	107.282(3)	111.726(5)	90	92.186(3)
V, Å^3	3680.8(2)	10443.7(10)	5508.5(3)	3680.8(6)
Z	4	8	4	4
T, K	100(2)	100(2)	100(2)	100(2)
ρ calcd, g cm^{-3}	1.404	1.371	1.387	1.463
refl. collected/$2\Theta_{max}$	67120/75.00	60105/50.00	50902/60.00	72671/60
unique refl./$I > 2\sigma(I)$	9662/7362	9183/6564	8015/5658	72671/10733
no. of params/restr.	222/0	597/9	339/0	451/0
λ, Å/μ(Kα), cm^{-1}	0.71073/6.40	0.71073/6.71	0.71073/5.12	0.71073/6.85
R1 [a]/goodness of fit [b]	0.0423/1.017	0.0607/1.034	0.0412/1.005	0.0495/1.020
wR2 [c] ($I > 2\sigma(I)$)	0.0911	0.1207	0.0728	0.0817
residual density, e Å^{-3}	+0.55/−0.88	+0.97/−0.96	+0.42/−0.39	+0.47/−0.44

[a] Observation criterion: $I > 2\sigma(I)$. R1 = $\sum||F_o| - |F_c||/\sum|F_o|$. [b] GooF = $[\sum[w(F_o^2 - F_c^2)^2]/(n-p)]^{1/2}$. [c] wR2 = $[\sum[w(F_o^2 - F_c^2)^2]/\sum[w(F_o^2)^2]]^{1/2}$ where $w = 1/\sigma^2(F_o^2) + (aP)^2 + bP$, $P = (F_o^2 + 2F_c^2)/3$.

synthesized according to procedures described in the literature: $[V(pdt)_3]^0$ (**1a**);[4] $[NEt_4][V(pdt)_3]$ (**1b**);[4] $[PPh_4]_2[V(mnt)_3]$ (**2c**);[23] $[PPh_4]_2[V(bdt)_3]$ (**3c**);[7] $[PPh_4]_2[V(tdt)_3]$ (**4c**);[7] $[V(edt)_3]^0$ (**5a**);[2] $[V(dtc)_3]^0$ (**6**).[35]

$[NEt_4]_2[V(pdt)_3]$ (1c). A solution of **1b** (100 mg; 0.110 mmol) in tetrahydrofuran (thf, 8 mL) under an Ar atmosphere was treated with sodium amalgam (10%; 27 mg; 0.117 mmol) and stirred for 30 h. The resultant sea-green reaction mixture was filtered on to a methanol (10 mL) solution containing NEt_4Br (28 mg; 0.133 mmol) that yielded a crystalline precipitate. The solid was collected, washed with methanol, and dried under vacuum. Yield: 47 mg (39%). The compound has been previously characterized in ref 2. Anal. Calcd for $C_{58}H_{70}N_2S_6V$: C, 67.08; H, 6.79. Found: C, 67.26; H, 6.68.

$[PPh_4][V(bdt)_3]$ (3b). A 50 mL Schlenk flask was charged with dry, deoxygenated tetrahydrofuran (10 mL), benzene-1,2-dithiol (115 μL, 0.999 mmol), and *n*-butyllithium (1.6 M solution in hexanes; 1.24 mL; 1.99 mmol) and stirred for 5 min at ambient temperature. The solvent was removed under vacuum after which an *aerated* tetrahydrofuran (10 mL) solution of $VCl_3(thf)_2$ (100 mg; 0.332 mmol) was added to the residue and stirred for 1 h. The resultant dark blue reaction mixture was filtered in air on to a methanol (15 mL) solution containing PPh_4Br (278 mg; 0.663 mmol). The resultant ink blue precipitate was collected by vacuum filtration, washed with methanol, then ether, and dried in vacuo. Yield: 68 mg (25%). Anal. Calcd for $C_{42}H_{32}PS_6V$: C, 62.20; H, 3.97. Found: C, 62.06; H, 4.44.

$[PPh_4][V(tdt)_3]$ (4b). The compound was prepared following the procedure described above using toluene-3,4-dithiol (132 μL; 0.996 mmol). Yield: 121 mg (43%). Anal. Calcd for $C_{45}H_{38}PS_6V$: C, 63.36; H, 4.49. Found: C, 62.77; H, 5.02.

X-ray Crystallographic Data Collection and Refinement of the Structures. Single crystals of compounds **1a**, **1b**·$2CH_2Cl_2$, **2c**, and **3b** were coated with perfluoropolyether, picked up with nylon loops and were immediately mounted in the nitrogen cold stream of a Bruker-Nonius Kappa-CCD diffractometer equipped with a Mo-target rotating-anode X-ray source. Graphite monochromated Mo−Kα radiation (λ = 0.71073 Å) was used throughout. Final cell constants were obtained from least-squares fits of all measured reflections. Intensity data were corrected for absorption using intensities of redundant reflections with the program SADABS.[38] The structures were readily solved by Patterson methods and subsequent difference Fourier techniques. The Siemens ShelXTL[39] software package was used for solution and artwork of the structures, ShelXL97[40] was used for the refinement. All non-hydrogen atoms were anisotropically refined, and hydrogen atoms were placed at calculated positions and refined as riding atoms with isotropic displacement parameters. Crystallographic data of the compounds are listed in Table 2. A dichloromethane molecule in **1b** was found to be severely disordered in a solvent channel. A split atom model with restrained C−Cl and Cl−Cl distances (DFIX) was refined giving an occupation ratio of 0.62:0.38. Equal anisotropic displacement parameters were assigned to the corresponding split atoms using the EADP instruction of ShelXL97.

X-ray Absorption Spectroscopy. All data were measured at the Stanford Synchrotron Radiation Lightsource under ring conditions of 3.0 GeV and 60−100 mA. S K-edge data were measured using the 54-pole wiggler beamline 6−2 or 4−3. A fully tuned Si(111) monochromator was utilized for energy selection, and a Ni-coated mirror was used for rejection of higher harmonics. All samples were measured at room temperature as fluorescence spectra using a Lytle detector. Samples were ground finely and dispersed as thinly as possible on Mylar tape to minimize the possibility of fluorescence saturation effects. Data represent 2−3 scan averages. All samples were monitored for photoreduction throughout the course of data collection. The S K-edge energy was calibrated using the S K-edge spectra of $Na_2S_2O_3 \cdot 5H_2O$, run at intervals between sample scans. The maximum of the first pre-edge feature in the spectrum was fixed at 2472.02 eV. A step size of 0.08 eV was used over the edge region. Data were averaged, and a smooth background was removed from all spectra by fitting a polynomial to the pre-edge region and subtracting this polynomial from the entire spectrum. Normalization of the data was accomplished by fitting a flattened polynomial or straight line to the postedge region and normalizing the postedge to 1.0.

V K-edge XAS data were measured using the focused 20-pole wiggler beamline 7−3. A Si(220) monochromator was utilized for energy selection, and a harmonic rejection mirror was present to minimize higher harmonic components in the X-ray beam. The solid samples were prepared as a dilute matrix in boron nitride, pressed into a pellet and sealed between 38 μm Kapton tape windows in a 1 mm aluminum spacer. Solution samples were prepared at ~3 mM concentrations in thf.

(38) Sheldrick, G. M. *SADABS, Bruker-Siemens Area Detector Absorption and Other Corrections*, Version 2006/1; Universität Göttingen: Göttingen, Germany, 2006.

(39) *ShelXTL 6.14*; Bruker AXS Inc.: Madison, WI, 2003.

(40) Sheldrick, G. M. *ShelXL97*; Universität Göttingen: Göttingen, Germany, 1997.

The sample of **2b** was prepared by controlled potential coulometry at 20 °C in an acetonitrile solution containing 0.10 M $[N(n\text{-}Bu)_4]PF_6$. Samples were maintained at 10 K during data collection by using an Oxford Instruments CF1208 continuous flow liquid helium cryostat. Data were measured in the transmission mode for solid samples. A 30-element solid state Ge detector was utilized for the detection of fluorescence from solution samples. Internal energy calibrations were performed by simultaneous measurement of the V reference foil places between a second and third ionization chamber with the inflection point assigned at 5465 eV. Data represent 2−4 scan averages and were processed by fitting a second-order polynomial to the pre-edge region and subtracting this background from the entire spectrum. A three-region cubic spline was used to model the smooth background above the edge. The data were normalized by subtracting the spline and normalizing the post-edge to 1.0. Fits to the pre-edges modeled by pseudo-Voigt lines were carried out using the program EDG_FIT[41] with a fixed 1:1 ratio of Lorentzian to Gaussian contributions.

Other Physical Measurements. Electronic absorption spectra of complexes from the spectroelectrochemical measurements were recorded on a HP 8452A diode array spectrophotometer (200−1100 nm). Cyclic voltammograms were recorded with an EG&G potentiostat/galvanostat. Variable temperature (4−300 K) magnetization data were recorded in a 1 T magnetic field on a SQUID magnetometer (MPMS Quantum Design). The experimental magnetic susceptibility data were corrected for underlying diamagnetism using tabulated Pascal's constants. ^{1}H NMR spectra were recorded on a Varian Mercury 400 MHz instrument at ambient temperature. X-band EPR spectra were recorded on a Bruker ESP 300 spectrometer and simulated with XSophe[42] distributed by Bruker Biospin GmbH. Elemental analyses were performed by H. Kolbe at the Mikroanalytischen Labor in Mülheim an der Ruhr, Germany.

Calculations. All DFT calculations were performed with the ORCA program.[43] The complexes were geometry optimized using the B3LYP functional.[44] The all-electron basis sets were those reported by the Ahlrichs group.[45] Triple-ξ-quality basis sets with one set of polarization functions (def2-TZVP) were used for the metal vanadium and the sulfur atoms. The remaining atoms were described by slightly smaller polarized split-valence def2-SV(P) basis sets that are double-ξ-quality in the valence region and contain a polarizing set of d functions on the non-hydrogen atoms. Auxiliary basis sets used to expand the electron density in the calculations were chosen to match the orbital basis. The self-consistent field calculations were tightly converged (1×10^{-8} E_h in energy, 1×10^{-7} E_h in the density charge, and 1×10^{-7} in the maximum element of the DIIS[46] error vector). The geometry search for all complexes was carried out in redundant internal coordinates without imposing geometry constraints. The coordinates for the sequentially (5°) twisted molecules of **5a** and $[V(SQ)_3]$, where SQ = benzosemiquinone(1−), were generated with the Z-matrix editor in Molden.[47] Single point energies were run using the same conditions detailed for the optimization. We used the broken symmetry (BS) approach to describe our computational results for the monoanionic compounds (**1b**, **2b**, **3b**), octahedral **1a**, and its dioxolene analogue, $[V(SQ)_3]$.[48] We adopt the following notation: the given system was divided into two fragments. The notation BS(m,n) refers then to a broken symmetry state with m unpaired α-spin electrons essentially on fragment 1 and n unpaired β-spin electrons localized on fragment 2. In most cases, fragments 1 and 2 correspond to the metal and the ligands, respectively. In this notation the standard high-spin, open-shell solution is written as BS($m + n$,0). The BS(m,n) notation refers to the initial guess to the wave function. The variational process does, however, have the freedom to converge to a solution of the form BS($m - n$,0) in which effectively the $n\beta$-spin electrons pair up with $n < m\alpha$-spin electrons on the partner fragment. Such a solution is then a standard $M_s \cong (m - n)/2$ spin-unrestricted Kohn−Sham solution. As explained elsewhere,[49] the nature of the solution is investigated from the corresponding orbital transformation (COT) which, from the corresponding orbital overlaps, displays whether the system should be described as a spin-coupled or a closed-shell solution. Corresponding[49] and canonical orbitals and density plots were obtained using Molekel.[50]

Time-dependent (TD-DFT) calculations of the vanadium and sulfur K-pre-edges were conducted as previously described.[26,34,51−53] For all complexes, a single point, spin unrestricted ground state DFT calculation, starting from the optimized coordinates, was performed. Here, a fully uncontracted CP(PPP) basis set was employed for vanadium,[54] while the same basis sets as described previously were used for the other atoms.[45] TD-DFT calculations[55] were then performed allowing for only transitions from the vanadium 1s orbital.[52] For the S K-edge spectra, the six sulfur 1s orbitals were localized using the Pipek−Mezey criteria,[56] and the TD-DFT equations were solved individually for each sulfur atom, excluding all but excitations originating from the sulfur 1s orbital.[30,51] The absolute calculated transition energies are consistently underestimated because of shortcomings in the ability of DFT to model potentials near the nucleus. This results in the deep 1s orbitals being too high in energy relative to the valence, thus requiring a constant shift for a given absorber.[51,52] It was established that constant shifts of +116.3 eV for the V K-edge and +57.41 eV for S K-edge are required for this level of theory. Plots were obtained using "orca_mapspc" with a line broadening of 1.0 eV for V K-edges and 0.8 eV for S K-edges. Despite the inherent restrictions in describing open-shell systems with a single determinantal reference wave function,[30,52,57] we have found this method is quite effective at predicting the energy and relative intensities for transitions originating from the V or S 1s orbital for the vanadium tris(dithiolene) monoanions.

(41) George, G. N. *EXAFSPAK & EDG_FIT*; Stanford Synchrotron Radiation Laboratory, Stanford Linear Accelerator Center, Stanford University: Palo Alto, CA, 2000.
(42) Hanson, G. R.; Gates, K. E.; Noble, C. J.; Griffin, M.; Mitchell, A.; Benson, S. *J. Inorg. Biochem.* **2004**, *98*, 903.
(43) Neese, F. *Orca, an Ab Initio, Density Functional and Semiempirical Electronic Structure Program Package*, version 2.7, revision 1523; Universität Bonn: Bonn, Germany, 2009.
(44) (a) Becke, A. D. *Phys. Rev. A* **1988**, *38*, 3098. (b) Becke, A. D. *J. Chem. Phys.* **1993**, *98*, 5648. (c) Lee, C. T.; Yang, W. T.; Parr, R. G. *Phys. Rev. B* **1988**, *37*, 785.
(45) Weigend, F.; Ahlrichs, R. *Phys. Chem. Chem. Phys.* **2005**, *7*, 3290.
(46) (a) Pulay, P. *Chem. Phys. Lett.* **1980**, *73*, 393. (b) Pulay, P. *J. Comput. Chem.* **1992**, *3*, 556.
(47) Schaftenaar, G.; Noordik, J. H. *J. Comput.-Aided Mol. Des.* **2000**, *14*, 123.
(48) (a) Noodleman, L. *J. Chem. Phys.* **1981**, *74*, 5737. (b) Noodleman, L.; Case, D. A.; Aizman, A. *J. Am. Chem. Soc.* **1988**, *110*, 1001. (c) Noodleman, L.; Davidson, E. R. *Chem. Phys.* **1986**, *109*, 131. (d) Noodleman, L.; Norman, J. G.; Osborne, J. H.; Aizman, A.; Case, D. A. *J. Am. Chem. Soc.* **1985**, *107*, 3418. (e) Noodleman, L.; Peng, C. Y.; Case, D. A.; Monesca, J. M. *Coord. Chem. Rev.* **1995**, *144*, 199.
(49) Neese, F. *J. Phys. Chem. Solids* **2004**, *65*, 781.
(50) *Molekel, Advanced Interactive 3D-Graphics for Molecular Sciences*; Swiss National Supercomputing Center; http://www.cscs.ch/molkel.
(51) DeBeer George, S.; Petrenko, T.; Neese, F. *Inorg. Chim. Acta* **2008**, *361*, 965.
(52) DeBeer George, S.; Petrenko, T.; Neese, F. *J. Phys. Chem. A* **2008**, *112*, 12936.
(53) Berry, J. F.; DeBeer George, S.; Neese, F. *Phys. Chem. Chem. Phys.* **2008**, *10*, 4361.
(54) Neese, F. *Inorg. Chim. Acta* **2002**, *337*, 181.
(55) Neese, F.; Olbrich, G. *Chem. Phys. Lett.* **2002**, *362*, 170.
(56) Pipek, J.; Mezey, P. G. *J. Chem. Phys.* **1989**, *90*, 4916.
(57) Herebian, D.; Wieghardt, K.; Neese, F. *J. Am. Chem. Soc.* **2005**, *125*, 10997.

Results

Syntheses and Characterization. Solid materials of complexes shown in Scheme 2 have been synthesized according to procedures described in the literature (see Experimental Section). Compounds **3b** and **4b** were prepared in slightly aerated thf using a 3:1 ligand/metal molar ratio. Filtering the reaction mixture in air and addition of a suitable countercation, led to the isolation of dark ink blue solids in reasonable yields. These were characterized by NMR, mass spectrometry, elemental analysis, and for **3b**, X-ray crystallography. From temperature dependent (4−300 K) magnetic susceptibility measurements, a doublet ground state ($S = {}^1/_2$) was confirmed for neutral complexes **1a** and **5a**, and dianions in **1c**, **3c**, and **4c**. The singlet ground state of the monoanions in **1b**, **3b**, and **4b** are apparent from their "normal" proton NMR spectra recorded at ambient temperature.

EPR Spectroscopy. Figure 1 shows the X-band EPR spectra of **1a** and **1c** recorded in CH_2Cl_2 solution at ambient temperature, and Table 3 summarizes the EPR data for neutral species **1a**, **5a**, and the dianions **1c**, **2c**, **3c**, **4c**, and **5c**. The fluid solution spectra of **1a** and **1c** are nearly indistinguishable, and as proposed by Kwik and Stiefel,[15] clearly confirm the common $(d_{z^2})^1$ ($S = {}^1/_2$) ground state[5,6] for the neutral and dianionic species. The line shape pattern has been successfully simulated using an isotropic liquids model that incorporates parameters to model tumbling rates of the molecules in solution (Supporting Information, Table S1). As is shown below, the spin density localized on the V(IV) ion is very similar (+1.375 and +1.404) for **1a** and **1c**, respectively.

The frozen solution spectra for all $S = {}^1/_2$ species are characterized by an axial 8-line spectrum with minute g-anisotropy that is nearly isotropic for the neutral complexes **1a** and **5a**. The dianionic species with aromatic dithiolates (**3c** and **4c**) have a greater g-anisotropy than their olefinic counterparts (**1c**, **2c**, **5c**). In contrast, each spectrum is dominated by a large, highly anisotropic magnetic hyperfine interaction arising from the ^{51}V nucleus ($I = {}^7/_2$, 100% natural abundance). Here, the spectral width is determined by the large $A_\perp$ (A_{xx}, A_{yy}) hyperfine components; small perturbations in the frozen solution structure of the complexes leads to slight drift away from perfect axial symmetry in the spectra. This heterogeneity gives rise to a line broadening that is maximized at the extremes of the spectrum. To accommodate this feature, we have employed a significant A-strain that has been successful in modeling this unique line shape (Supporting Information, Table S2). From our simulation of **2c**, we have obtained different spin Hamiltonian parameters than those derived from the single crystal study.[15] Kwik and Stiefel suggested that $A_\perp$ has a different sign to the much smaller $A_\parallel$ (A_{zz}). In their experiment, the large hyperfine component was easily distinguished and attributed to the perpendicular components; however, the significantly smaller $A_\parallel$ was not measurable, so it was assumed to be small and negative to give a better approximation to the isotropic hyperfine value. We have discovered that the value of $A_\parallel$ is small such that the sign (positive or negative) has negligible impact on the simulation. However, we have kept the A-tensor components with the same sign since it is better agreement with the isotropic hyperfine value. A similar result was reported for the previously published EPR parameters for **3c** and **4c**.[7]

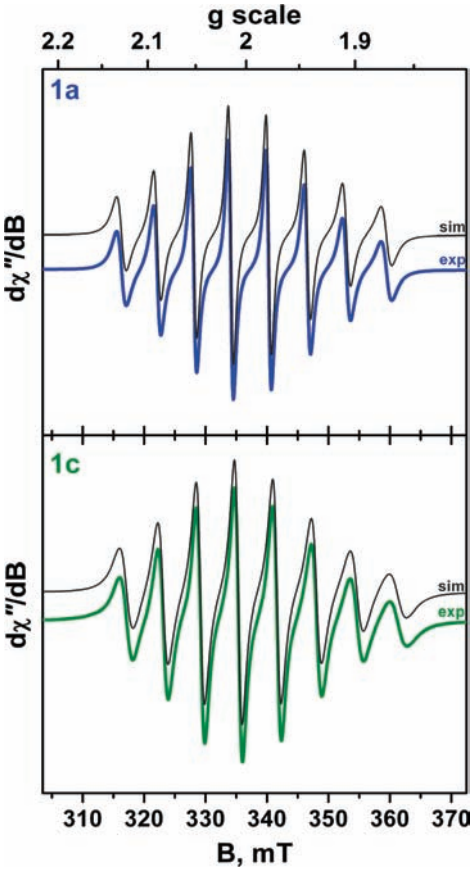

Figure 1. X-band EPR spectra of $[V(pdt)_3]^0$ (**1a**, top) and, $[V(pdt)_3]^{2-}$ (**1c**, bottom) in CH_2Cl_2 solutions at 293 K. Conditions: frequency 9.42 GHz; power 0.63 mW; modulation 0.5 mT. Simulations are shown in black and parameters are given in Table 3.

Magnetic Susceptibility. A magnetic moment of 2.78 μ_B for $[V(dtc)_3]$ (**6**) has been measured by using a Gouy balance (89−295 K).[36] We have repeated this measurement in the temperature range 4−300 K by using a SQUID magnetometer (Supporting Information, Figure S12). A temperature independent magnetic moment of 2.59 ± 0.02 μ_B with $g = 1.97$, a zero-field splitting parameter, $D = -10.4$ cm^{-1}, and a rhombicity, $E/D = 0.11$ were obtained from the simulation.

No information on the spin states of the tri- and tetraanions $[V(L)_3]^{3-/4-}$ are available in the literature which is a consequence of the fact that no salts containing these anions have been isolated as solid materials to date. Since the three dithiolene ligands exist in their lowest possible oxidation level in the dianionic species, $[V(mnt)_3]^{2-}$, it is quite natural to assume that further one-electron reductions of this species are a metal-centered processes generating $[V(mnt)_3]^{3-}$ with a central vanadium(III) ion (d^2, $S = 1$), and $[V^{II}(mnt)_3]^{4-}$ with a central vanadium(II) ion (d^3, $S = {}^3/_2$), respectively. The ν(CN) stretching frequency for the tetraanion has been examined using potential-modulation spectroelectrochemical techniques that facilitate measurement of the very short-lived tetraanionic complex.[11] The ν(CN) stretch was seen to decrease by 22 cm^{-1} upon reduction of the trianion to the tetraanion, and was attributed to

Table 3. EPR Spin Hamiltonian *g*-Tensor and ^{51}V ($I = {}^{7}/_{2}$, 100% Abundance) Magnetic Hyperfine Tensor ($A \times 10^{-4}$ cm^{-1})[a] Derived from Simulation of the Room Temperature and Frozen Solution (30 K) Spectra of the Neutral and Dianionic $S = {}^{1}/_{2}$ Complexes[b]

compound	g_{iso}	A_{iso}	g_x	g_y	g_z	$\langle g \rangle^c$	A_{xx}	A_{yy}	A_{zz}	$\langle A \rangle^d$
1a	1.991	−57.2	1.989	1.991	1.993	1.991	−83.0	−80.5	−5.0	−56.2
5a	1.990	−57.5	1.988	1.989	1.991	1.989	−84.0	−81.0	−8.0	−57.7
1c	1.983	−58.3	1.976	1.980	1.992	1.983	−87.0	−85.0	−4.0	−58.7
2c	1.982	−58.9	1.978	1.980	1.989	1.982	−88.0	−84.0	−3.0	−58.3
3c	1.980	−60.2	1.974	1.977	1.993	1.981	−89.0	−86.0	−2.0	−59.0
4c	1.980	−60.2	1.973	1.976	1.994	1.981	−88.0	−87.0	−3.0	−59.3
5c[e]			1.976	1.977	1.993	1.982	−89.0	−88.0	−2.0	−59.7

[a] The sign of the *A*-tensor is assumed to be negative owing to the dominant Fermi-contact contribution. [b] Experimental conditions are available in the Supporting Information, Tables S1 and S2. [c] $\langle g \rangle = (g_x + g_y + g_z)/3$. [d] $\langle A \rangle = (A_{xx} + A_{yy} + A_{zz})/3$. [e] Generated by controlled potential coulometry; no room temperature spectrum recorded.

Table 4. Selected Bond Distances (Å) and Twist (Θ, deg) and Fold Angles (α, deg) in **1a**, **1b**·$2CH_2Cl_2$, **2c**, and **3b**

		Complex **1a**			
V−S(1)	2.3467(3)	V−S(4)	2.3352(3)	V−S(31)	2.3500(3)
S(1)−C(2)	1.707(1)	S(4)−C(3)	1.700(1)	S(31)−C(32)	1.699(1)
C(2)−C(3)	1.394(2)	C(32)−C(32)′	1.404(2)		
Θ_1	5.4°	Θ_2	5.4°	Θ_3	3.2°
α	3.7°	α′	3.7°	α″	0.0°
		Complex **1b**·$2CH_2Cl_2$			
V−S(1)	2.331(1)	V−S(4)	2.327(1)	V−S(31)	2.338(1)
V−S(34)	2.318(1)	V−S(61)	2.313(1)	V−S(64)	2.346(1)
S(1)−C(2)	1.729(4)	S(4)−C(3)	1.725(4)	S(31)−C(32)	1.730(4)
S(34)−C(33)	1.741(4)	S(61)−C(62)	1.726(4)	S(64)−C(63)	1.732(4)
C(2)−C(3)	1.376(6)	C(32)−C(33)	1.369(6)	C(62)−C(63)	1.379(6)
Θ_1	0.3°	Θ_2	1.7°	Θ_3	0.3°
α	24.7°	α′	26.1°	α″	20.4°
		Complex **2c**			
V−S(1)	2.3637(6)	V−S(11)	2.3752(5)	V−S(14)	2.3632(5)
S(1)−C(2)	1.732(2)	S(11)−C(12)	1.730(2)		
C(2)−C(2)′	1.360(4)	C(12)−C(13)	1.363(3)		
Θ_1	33.9°	Θ_2	40.1°	Θ_3	40.1°
α	0.0°	α′	6.5°	α″	6.5°
		Complex **3b**			
V−S(1)	2.3700(8)	V−S(8)	2.3368(8)	V−S(11)	2.3407(8)
V−S(18)	2.3613(8)	V−S(21)	2.3370(8)	V−S(28)	2.3529(8)
S(1)−C(2)	1.740(3)	S(8)−C(7)	1.743(3)	C(2)−C(7)	1.408(4)
C(2)−C(3)	1.407(4)	C(3)−C(4)	1.387(4)	C(4)−C(5)	1.398(4)
C(5)−C(6)	1.380(4)	C(6)−C(7)	1.414(3)		
S(11)−C(12)	1.737(3)	S(18)−C(17)	1.734(4)	C(12)−C(17)	1.411(3)
C(12)−C(13)	1.408(4)	C(13)−C(14)	1.387(4)	C(14)−C(15)	1.399(4)
C(15)−C(16)	1.378(4)	C(16)−C(17)	1.412(4)		
S(21)−C(22)	1.739(2)	S(28)−C(27)	1.740(3)	C(22)−C(27)	1.413(3)
C(22)−C(23)	1.410(3)	C(23)−C(24)	1.377(4)	C(24)−C(25)	1.401(4)
C(25)−C(26)	1.380(4)	C(26)−C(27)	1.406(3)		
Θ_1	0.0°	Θ_2	2.9°	Θ_3	1.0°
α	22.5°	α′	21.6°	α″	23.6°

an increase in the occupancy of the predominately metal-based $5e'$ molecular orbitals (MOs) that led to increased π backbonding to the mnt ligands; a supposition corroborated by DFT calculations (see below).

Crystal Structure Determinations. The crystal structure of the neutral species [V(pdt)$_3$] has been solved by using single-crystal X-ray diffraction at room temperature.[5,6] The intensities of the reflections have been collected in 1966 by the then standard film techniques. Consequently, the average estimated standard deviations (esd) of the olefinic C−C, the C−S, and the V−S bonds of the five membered chelate rings V−S−C−C−S are quite large. These bond distances and their esds are reported to be as follows: C−C 1.46(2) Å, C−S 1.685(10) Å, V−S 2.337(4) Å.[5,6] We have reinvestigated this structure by using an automated four-circle diffractometer at 100(2) K. The results are summarized in Table 4, and Figure 2a shows the structure of a neutral molecule. As expected the average esd values are now significantly smaller: the av. olefinic C−C bond distance is observed at 1.399(2) Å, the C−S at 1.702(1) Å, and the V−S at 2.3440(3) Å. These values indicate a somewhat more reduced dithiolene ligand set as may have been implied from the room temperature structure. Overall, the agreement of these two structure determinations is exceptional, a testament to the high quality work performed in 1966. The VS_6 polyhedron is trigonal prismatic (av. $\Theta = 4.6°$); the average folding angle α is at 2.5°.

The structure of **1b**·$2CH_2Cl_2$ contains a monoanion $[V(pdt)_3]^{1-}$ and a well-separated tetraethylammonium cation (1:1) and two CH_2Cl_2 molecules of solvation.

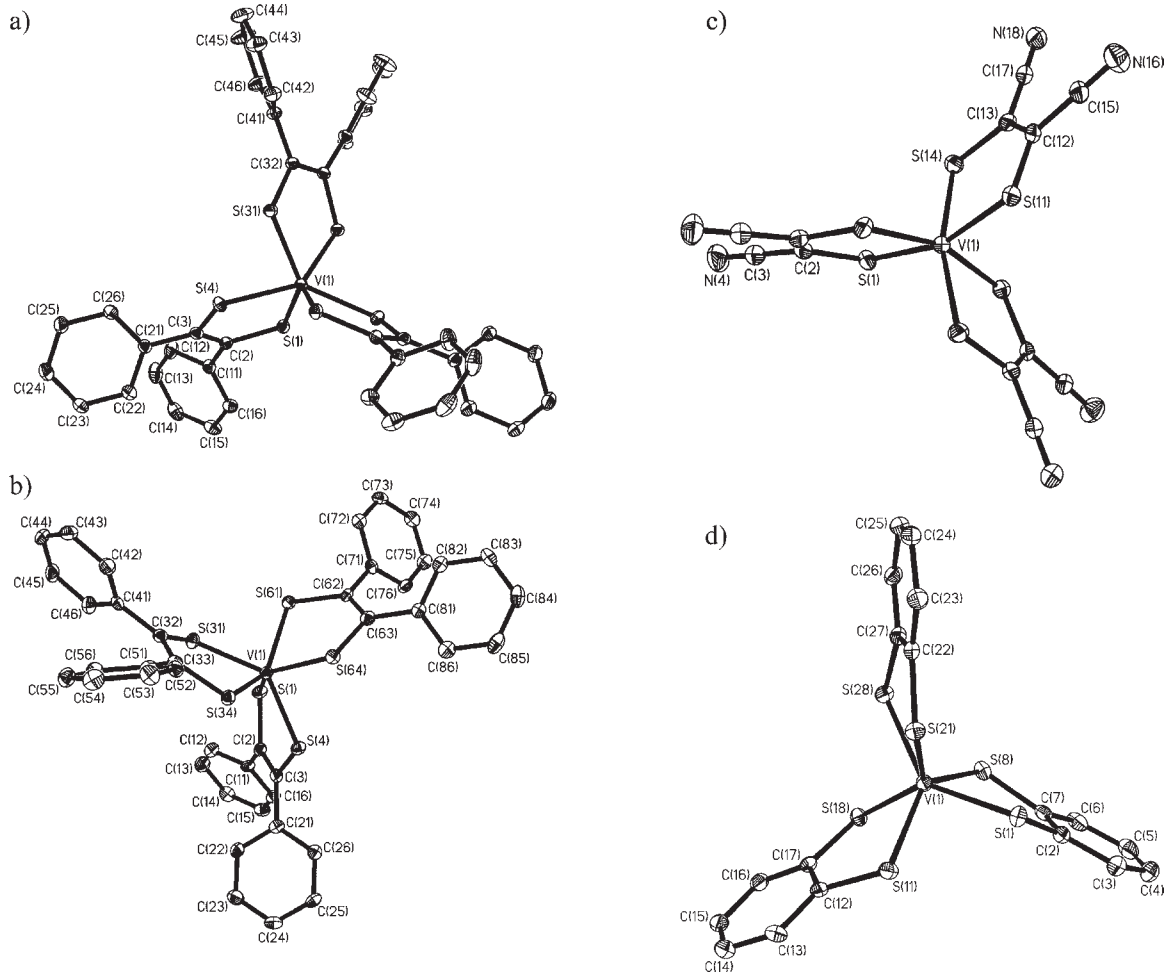

Figure 2. Structures of (a) the neutral molecule $[V(pdt)_3]$ in crystals of **1a**, (b) the monoanion $[V(pdt)_3]^{1-}$ in crystals of **1b**·$2CH_2Cl_2$, (c) the dianion $[V(mnt)_3]^{2-}$ in crystals of **2c**, and (d) the monoanion $[V(bdt)_3]^{1-}$ in crystals of **3b**.

The monoanion has not been structurally characterized previously, though this did not prevent Eisenberg, Gray, and co-workers from predicting a trigonal prismatic structure.[5,6] Figure 2b displays its structure, and Table 4 summarizes selected bond distances and angles. As anticipated, the VS_6 polyhedron is nearly perfectly trigonal prismatic (av. $\Theta = 0.8°$) as in **1a**. The average C−S bond length at 1.730(4) Å is longer than in **1a**, and the average olefinic C−C distance at 1.375(4) is slightly shorter than in **1a**, which indicates a lower average oxidation level of the three dithiolene ligands in **1b** than in **1a**. Thus, the one-electron reduction of **1a** appears to be a ligand-centered process: $[V^{IV}(L_3{}^{4-})]^0 + e \rightarrow [V^{IV}(L_3{}^{5-\bullet})]^{1-}$. This observation is corroborated by the nearly identical average V−S bond length in **1a** and **1b** of ∼2.336 Å.

The structure of the dianion in **2c** is shown in Figure 2c, and selected bond distances are given in Table 4. The structure of $[NMe_4]_2[V(mnt)_3]$ has been reported by Stiefel, Dori, and Gray in 1967.[16] Since the intensity data were collected by the multiple film equiinclination Weissenberg technique using Cu Kα radiation at ambient temperature, we have investigated the structure of **2c** at 100(2) K by using an automated four-circle diffractometer and Mo Kα radiation. The results of the two structure determinations are again reassuringly similar and demonstrate again the high quality of earlier structure determinations. The average C−S bond length of the ligands at 1.731(2) Å (old value from ref 16: 1.72 ± 0.02 Å) and the average olefinic C−C bond distance at 1.362(3) Å (old 1.33 ± 0.03 Å) are a clear indication of three dianionic dithiolato $(mnt)^{2-}$ ligands. These data are in excellent agreement with those reported for $[Fe^{III}(cyclam)(mnt)](BF_4)$,[33] which contains an unambiguous fully reduced mnt^{2-} ligand. As stated in ref 16 "the polyhedron described by these (six) sulfur atoms is by no means a regular one, but for some purposes it is usefully described as a very distorted octahedron." The three twist angles Θ of 33.9°, 40.1°, and 40.1° support this view. The average V−S bond length at 2.367 Å is close to those observed in **1a** and **1b** and is a structural indication that the metal oxidation state remains constant on going from the neutral, to the monoanion, and to the dianion in the $[V(L)_3]^z$ ($z = 0, 1-, 2-$) series. The structure of the monoanion $[V(bdt)_3]^{1-}$ in crystals of **3b** is shown in Figure 2d. Selected bond distances and angles are summarized in Table 4. The geometry of the three ligands is identical within experimental error. The average C−S bond length at 1.739 ± 0.01 Å is slightly shorter than in *S,S*-coordinated benzene-1,2-dithiolate dianions at ∼1.765 Å,[58] and

(58) (a) Ray, K.; Begum, A.; Weyhermüller, T.; Piligkos, S.; van Slageren, J.; Neese, F.; Wieghardt, K. *J. Am. Chem. Soc.* **2005**, *127*, 4403. (b) Ray, K.; Bill, E.; Weyhermüller, T.; Wieghardt, K. *J. Am. Chem. Soc.* **2005**, *127*, 5641.

Table 5. Redox Potentials (V) of Complexes Versus Fc^+/Fc[a]

complex[b]	$E^1_{1/2}$ 1+/0	$E^2_{1/2}$ 0/1−	$E^3_{1/2}$ 1−/2−	$E^4_{1/2}$ 2−/3−	$E^5_{1/2}$ 3−/4−	ref
1b	+0.68 irr	−0.17 r	−1.19 r	−2.21 qr		this work
2c		+1.12 irr	+0.13 r	−0.92 r	−2.09 r	this work
3c		+0.12 irr	−0.62 r	−1.92 r		this work
4c		+0.09 irr	−0.66 r	−1.93 r		this work
5a	+0.74 irr	−0.20 r	−1.01 r	−2.15 irr		this work
$[V(sdt)_3]^{1-}$[c]		−0.20 r	−1.13 r			59
$[V(tfd)_3]^{2-}$[d]		+0.82 irr	−0.39 r	−1.44 [e]		10
$[V(Cl_4\text{-}bdt)_3]^{2-}$[f]		+0.62 irr	−0.21 r	−1.35 r		10
$[V(dddt)_3]^{1-}$[g]		−0.08 r	−0.98 r	−1.91 r		12

[a] r = reversible; qr = quasi-reversible; irr = irreversible. [b] Recorded in CH_2Cl_2 solutions containing 0.1 M $[N(n\text{-}Bu)_4]PF_6$ at 25 °C using a scan rate of 100 mV s^{-1}. [c] Potentials converted by adding −0.46 V. Only the reversible processes were reported. [d] $(tfd)^{2-}$ = bis(trifluoromethyl)ethylenedithiolate. Potentials converted by adding −0.38 V. [e] Reversibility unknown. [f] $(Cl_4\text{-}bdt)^{2-}$ = 3,4,5,6-tetrachlorobenzene-1,2-dithiolate. Potentials converted by adding −0.38 V. [g] Potentials converted by adding −0.47 V.

may indicate the presence of a single oxidative hole distributed over three such ligands: $(L_3)^{5-\bullet}$. The average V−S bond distance is found at 2.350 ± 0.003 Å and is nearly identical with that found in neutral **1a** at 2.344 ± 0.001 Å and the monoanion in **1b** at 2.329 ± 0.003 Å. The similarity indicates that the oxidation state of the central vanadium ion is +IV in the neutral, the mono-, and the dianionic species. The VS_6 polyhedron in **3b** is trigonal prismatic with an average twist angle Θ of 1.3°. Interestingly, the average fold angle α at 22.6° is quite large and agrees well with other crystallographically characterized monoanions $[V(L)_3]^{1-}$ (Table 1).[8,12−14] In the neutral and dianionic species this angle α is significantly smaller.

Electro- and Spectroelectrochemistry. The electrochemistry of most complexes listed in Scheme 2 has been investigated in the past. Here, the cyclic voltammograms (CV) of complexes **1b**, **2c**, **3c**, **4c**, and **5a** have been recorded using standardized conditions in CH_2Cl_2 solutions containing 0.1 M $[N(n\text{-}Bu)_4]PF_6$ as supporting electrolyte at a glassy carbon working electrode and a scan rate of 100 mV s^{-1} at 22 °C. Table 5 summarizes the results. All redox potentials are referenced versus the ferrocenium/ferrocene (Fc^+/Fc) couple.

Figure 3 displays the CVs of **1a** and **2c**; those of **3c**, **4c**, and **5a** are shown in the Supporting Information, Figure S13. The CV of **1a** displays two reversible one-electron transfer waves at $E_{1/2}$ = −0.17, −1.19 V, and a quasi-reversible reductive wave at −2.21 V. In addition, an irreversible oxidative one-electron wave is observed at +0.68 V, the only available evidence for a putative monocation $[V(pdt)_3]^{1+}$ ($[\mathbf{1a}]^+$). Thus, couples $[V(L_3)]^{1+/0}$, $[V(L_3)]^{0/1-}$, $[V(L_3)]^{1-/2-}$, $[V(L_3)]^{2-/3-}$ are electrochemically accessible in CH_2Cl_2 solution for $[V(pdt)_3]^z$ complexes. The species **1a**, **1b**, **1c** are stable in solution and may be coulometrically generated. Their electronic spectra have been recorded and are shown in Figure 4 (top).

Similarly, the CV of **2c** displays a reversible one-electron oxidation wave and two fully reversible one-electron reduction waves[11,60] which correspond to the couples $[V(mnt)_3]^{1-/2-}$, $[V(mnt)_3]^{2-/3-}$, and $[V(mnt)_3]^{3-/4-}$. Interestingly, an irreversible wave at +1.12 V indicates that the neutral species $[V(mnt)_3]^0$ is not stable under these conditions. The electronic spectra of the mono-, di-, and trianions, $[V(mnt)]^{1-/2-/3-}$, are shown in Figure 4 (bottom). The corresponding spectra of the series $[V(bdt)_3]^{1-/2-/3-}$,

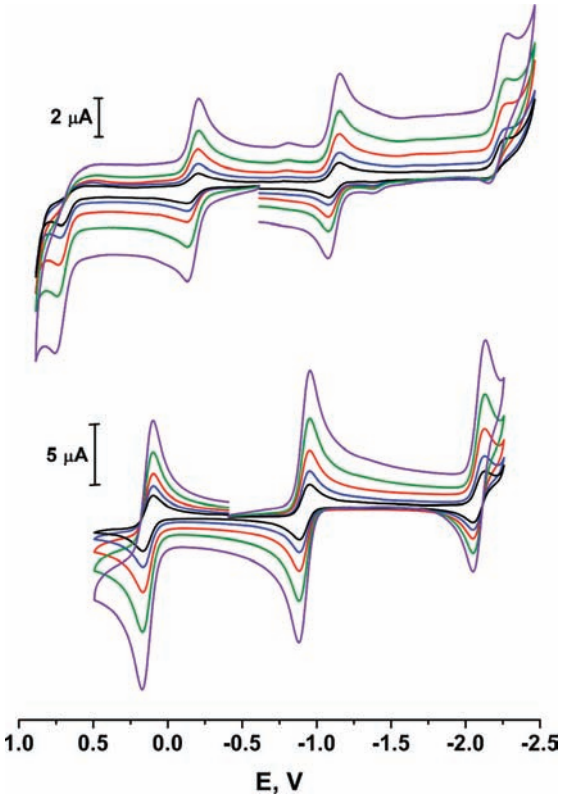

Figure 3. Cyclic voltammograms of **1a** (top) and **2c** (bottom) in CH_2Cl_2 solution (0.10 M $[N(n\text{-}Bu)_4]PF_6$ supporting electrolyte at 22 °C with a scan rates of 50, 80, 100, 200, and 500 mV s^{-1} (glassy carbon working electrode). Potentials are references versus the Fc^+/Fc couple.

$[V(tdt)_3]^{1-/2-/3-}$, and $[V(edt)_3]^{0/1-/2-}$ are displayed in the Supporting Information, Figures S14−S16. Table 6 summarizes the electronic spectra of all species recorded in CH_2Cl_2 solution (0.10 M $[N(n\text{-}Bu)_4]PF_6$) at −25 °C.

X-ray Absorption Spectroscopy (XAS). V K-Edge XAS. The V K-edge XAS data for complexes **1a**, **1b**, **2c**, and **6** are shown in Figure 5. Table 7 summarizes the 1s → 3d pre-edge energies and the 1s → 4p rising edge energies for **1a**, **1b**, **2b**, **2c**, **4c**, **5a**, and **6**; their spectra are displayed in the Supporting Information, Figure S17. In some cases, an additional transition is observed, which may be attributed to a formally two-electron 1s to 4p + LMCT shake-down transition[61] or it could reflect a transition to an

(59) Boyde, S.; Garner, C. D.; Joule, J. A.; Rowe, D. J. *Chem. Commun.* **1987**, 800.
(60) Best, S. P.; Clark, R. J. H.; McQueen, R. C. S.; Walton, J. R. *Inorg. Chem.* **1988**, *27*, 884.
(61) Solomon, E. I.; Hedman, B.; Hodgson, K. O.; Dey, A.; Szilagyi, R. K. *Coord. Chem. Rev.* **2005**, *249*, 97.

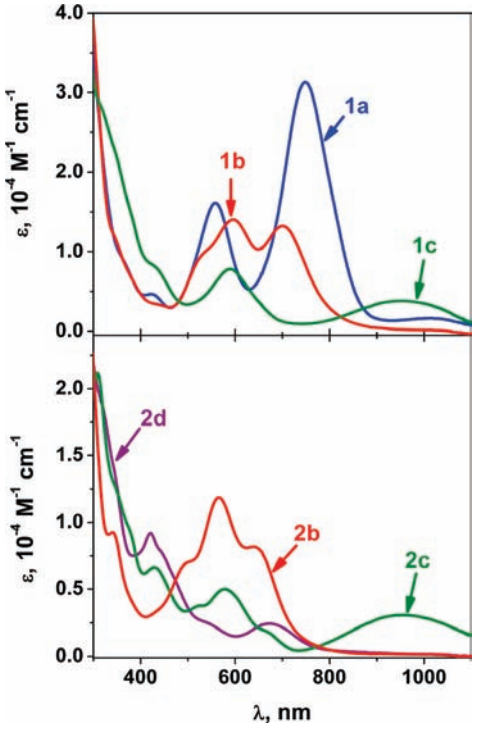

Figure 4. Electronic spectra of electrochemically generated neutral, monoanionic, and dianionic $[V(pdt)_3]^z$ (z = 0, 1−, 2−) species (top) and of mono-, di-, and trianionic $[V(mnt)_3]^z$ (z = 1−, 2−, 3−) (bottom) in CH_2Cl_2 (0.10 M $[N(n\text{-}Bu)_4]PF_6$) at −25 °C.

Table 6. Electronic Spectra of Electrochemically Generated Species in CH_2Cl_2 Solutions Containing 0.1 M $[N(n\text{-}Bu)_4]PF_6$, at −25 °C

complex	λ_{max}, nm (ε, 10^4 M^{-1} cm^{-1})
1a	1014(0.16), 783 (3.13), 558(1.61), 421(0.47), 352(sh, 1.02)
1b	700(1.32), 597(1.40), 545(sh, 1.04), 421(sh, 0.36), 340(sh, 1.25)
1c	955(0.38), 637(sh, 0.47), 590(0.78), 420(sh, 0.85), 312(sh, 2.87)
2b	639(0.82), 566(1.19), 508(sh, 0.71), 386(sh, 0.38), 341(0.93)
2c	954(0.31), 658(sh, 0.20), 578(0.50), 527(0.38), 430(0.67), 372(sh, 0.982), 339(sh, 1.34), 308(sh, 2.12)
2d	672(0.24), 530(sh, 0.27), 443(sh, 0.78), 421(0.92), 339(sh, 1.48)
3b	874(sh, 0.27), 670(sh, 0.88), 605(0.98), 519(0.90), 460(sh, 0.64), 366(sh, 309), 303(sh, 1.38)
3c	878(0.42), 681(sh, 0.46), 553(0.97), 426(0.85), 327(1.39)
3d	891(0.51), 552(0.90), 458(sh, 0.56), 423(1.05), 331(1.85)
4b	871(sh, 0.31), 700(0.89), 606(0.94), 528(0.93), 457(0.62), 367(sh, 0.35), 305(1.44)
4c	900(0.46), 559(0.82), 428(0.94), 332(1.66)
5a	911(0.05), 656(0.40), 513(0.49), 405(0.14), 351(0.23), 304(0.21)
5b	639(sh, 0.21), 576(0.40), 526(0.29), 363(0.21), 293(sh, 0.29)
5c	1010(0.09), 587(0.21), 422(sh, 0.12), 381(0.21), 311(0.34)
5d	905(0.23), 564(1.19), 423(0.62), 410(sh, 0.60), 325(1.64)

unoccupied ligand orbital with significant metal 4p character. The latter appears to be the case for compounds with $(mnt)^{2-}$ and $(dtc)^{1-}$ ligands as witnessed in Cr, Mn, and Fe analogues.[26,62] In many cases, this renders oxidation level assignment based on the rising edge inflection point ambiguous. Pre-edge energies are dominated by ligand field contributions. For a given tris(dithiolene) ligand set the ligand field will increase with increasing oxidation state of the vanadium center. Thus, the pre-edge energy provides a useful marker for the metal oxidation state. The V K-pre-edge energies for the two

(62) Milsmann, C.; Sproules, S.; Bill, E.; Weyhermüller, T.; DeBeer George, S.; Wieghardt, K. *Chem.—Eur. J.* **2010**, *16*, 3628.

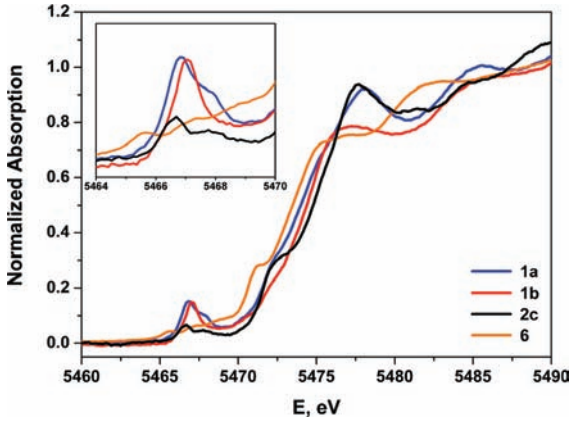

Figure 5. Comparison of the normalized V K-edge XAS spectra of **1a** (blue), **1b** (red), **2c** (black), and **6** (orange). The inset shows an expansion of the pre-edge region.

Table 7. Vanadium K-Edge Data for Both Solid and Solution Samples

compound	pre-edge[a]	area[b]	shakedown + LMCT[a]	rising-edge[a]
1a	5466.9 5467.6	0.31		5473.9
1a (soln)	5466.9 5467.6	0.24		5473.7
1b	5467.0	0.22		5473.7
1b (soln)	5467.1	0.16		5473.5
2b (soln)[c]	5467.2	0.23	5472.8	5474.8
2c	5466.7 5467.8	0.11	5472.9	5475.0
2c (soln)	5466.7 5467.9	0.13	5472.9	5475.5
4c	5466.7 5467.9	0.10		5473.9
5a	5466.8 5467.8	0.16	5470.8	5474.2
6	5465.7 5467.4	0.13	5471.5	5473.1

[a] In eV. The value is determined from the inflection point of the rising edge. [b] Area estimated by integrating the pre-edge region. [c] Generated by controlled potential coulometry in an acetonitrile solution containing 0.1 M $[N(n\text{-}Bu)_4]PF_6$ at 20 °C.

members $[V(pdt)_3]^{0,1-}$ of the electron transfer series are identical within experimental error at 5466.9 ± 0.2 eV. Interestingly, the pre-edge energy for **2c** at 5466.7 ± 0.2 eV is also very similar and indicates that the oxidation state of the vanadium ion is identical in the neutral, the monoanion, and the dianion regardless of the exact nature of the dithiolene ligand. The same is true for **4c** and **5a**. It is also important to note that the energy and the intensity of the V K-pre-edge peak of *solid* and *solution* samples of **1a**, **1b**, and **2c** are nearly identical (Supporting Information, Figure S18), clearly indicating the trigonal prismatic (**1a**, **1b**) and distorted octahedral (**2c**) geometries of the VS_6 polyhedra are retained in solution. The inset of Figure 5 displays the pre-edge peaks for **1a**, **1b**, and **2c**. $[V(dtc)_3]^0$ (**6**) is a distorted octahedral complex containing a genuine V^{III} ion (d^2, S = 1). Its V K-edge spectrum is also shown in Figure 5, and the data are given in Table 7. The pre-edge energy of **6** at 5465.7 eV is ∼1.0 eV lower in energy than is observed for all [tris(dithiolene)vanadium]$^{0,1-,2-}$ species. Note that **6** also displays the lowest rising-edge energy of all complexes, which is evidence that the oxidation state of the central vanadium

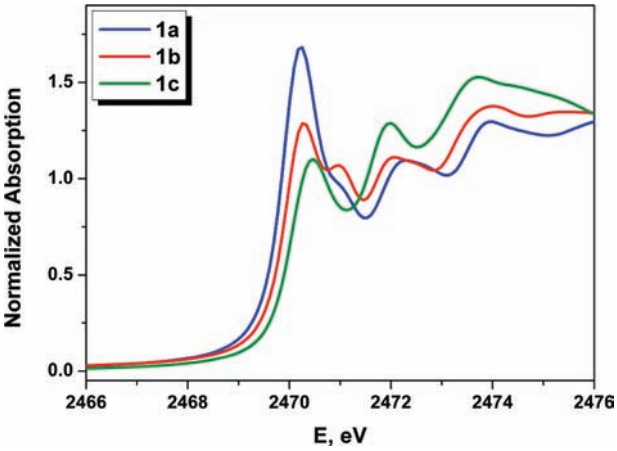

Figure 6. Comparison of the normalized S K-edge XAS spectra of **1a** (blue), **1b** (red), and **1c** (green).

ion in the [tris(dithiolene)vanadium]^z (z = 0, 1−, 2−) series is +IV comprising a d^1 ($S = {}^1/_2$) electronic configuration whereas in **6** it is +III (d^2, $S = 1$).

In the course of this study, we have evidenced a clear spectroscopic marker for the complex geometry; that is, the intensity of the V K-pre-edge peak. The transition intensity, defined as the area under the peak (Table 7), is 2−3 times greater for trigonal prismatic **1a** and **1b** than near octahedral **2c** and **6**, as seen in the inset of Figure 5. Electric quadrupole allowed 1s → 3d transitions gain intensity through 4p mixing into the 3d orbitals.[63] For coordination complexes with inversion symmetry, such as octahedral, mixing is forbidden; however, distortions toward a non-centrosymmetric geometry leads to increased vanadium 3d−4p mixing. In six-coordinate systems, this is maximized in a trigonal prism, and as is shown below, the calculated V 4p content of the 5e' MOs is ∼4% for trigonal prismatic **1a** and **1b**, whereas it is a meager 0.6% in **2c** and 0.4% in **6**. It is fortuitous that the long core-hole lifetime for the V K-edge sufficiently narrows the spectral line width such that the pre- and rising-edge portions of the spectrum are well separated. This feature does not occur for the heavier elements, such as Mo and Re, where the pre-edge transitions are not sufficiently resolved from the rising-edge.[34]

Armed with this knowledge, we measured the V K-edge of **2b** prepared by coulometric oxidation of **2c** in an acetonitrile solution containing 0.1 M [N(n-Bu)$_4$]PF$_6$ at 20 °C. Its pre-edge energy at 5467.2 ± 0.2 eV is only 0.5 eV higher in energy that the corresponding dianion, and 0.1 eV than **1b**. Moreover, the peak intensity matches that for **1b** (Supporting Information, Figure S19) such that in the absence of crystallographic characterization, **2b**, like all other characterized vanadium tris(dithiolene) monoanions, is trigonal prismatic.

Sulfur K-Edge XAS. Figure 6 shows a comparison of the experimental S K-edge spectra of the neutral complex, the corresponding monoanion, and of the dianion, namely, $[V(pdt)_3]^{0,1-,2-}$, in crystals of **1a**, **1b**, and **1c**; the pseudo-Voigt deconvoluted spectra are displayed in Figure 7. The deconvoluted spectra of **2c**, **3c**, **4c**, and **6** are shown in the Supporting Information, Figures S20−S23.

(63) Shulman, R. G.; Yafet, Y.; Eisenberger, P.; Blumberg, W. E. *Proc. Natl. Acad. Sci. U.S.A.* **1976**, *73*, 1384.

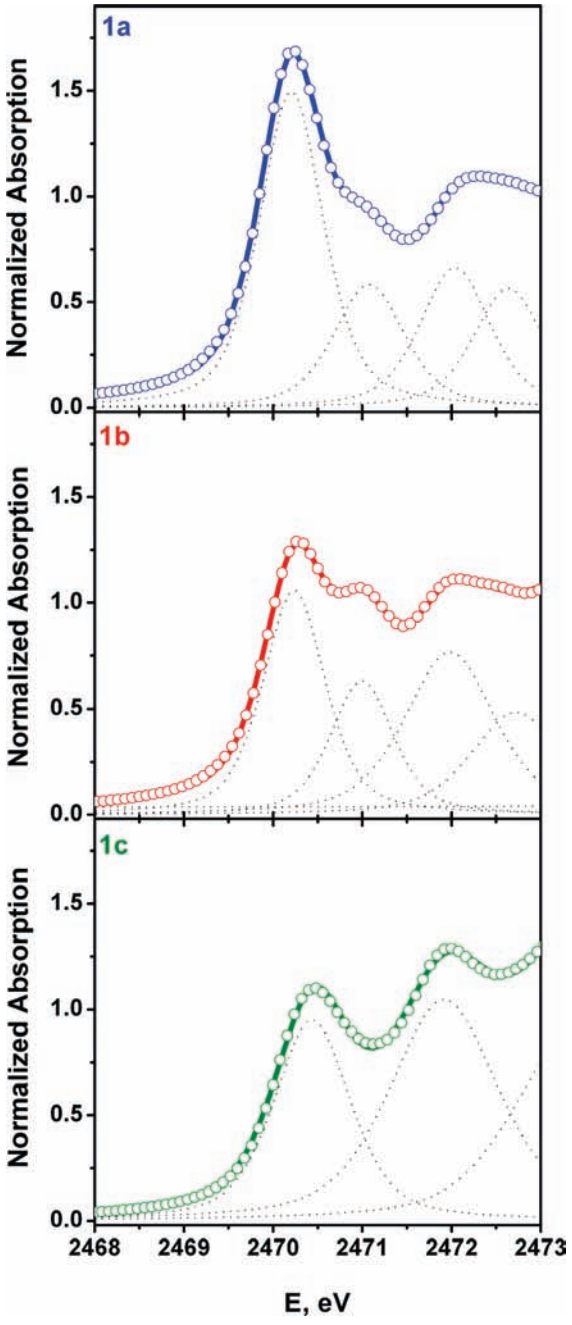

Figure 7. Pseudo-Voigt deconvolution of the S K-edge spectra of **1a**, **1b**, and **1c**. Circles represent the experimental data; dotted lines the pseudo-Voigt peaks; and the solid line is the sum of the fit.

The results of the analysis of the pre-edge and near-edge peak energies are presented in Table 8.

The spectra of the dianions in crystals of **1c**, **2c**, **3c**, and **4c** display a single pre-edge peak at 2470.44; 2470.54; 2470.36, and 2470.37 eV, respectively, and a higher-energy near-edge peak at 2471.92, 2472.02, 2471.77; 2471.70, respectively (Supporting Information, Figure S24, top). Only the spectrum of **2c** shows a third peak at intermediate energy at 2471.47 eV; this has been witnessed before in other tris(mnt) complexes.[26] The spectrum of **6** has a small shoulder at 2470.81 eV and a more intense second pre-edge peak at 2472.07 eV (Supporting Information, Figure S25, top). It is now very important that only the spectra of neutral **1a** and monoanionic **1b**

Table 8. Sulfur K-Edge XAS Energy Positions (eV)

compound	pre-edge	area[a]	near-edge[b]
1a	2470.21	1.272	2472.64
	2471.08	0.549	
	2472.04	0.620	
1b	2470.24	0.877	2472.72
	2471.00	0.528	
	2471.98	0.922	
1c	2470.44	0.967	2473.35
	2471.92	1.518	
2c	2470.54	0.901	2473.24
	2471.47	0.340	
	2472.02	0.890	
3c	2470.36	1.032	2472.65
	2471.77	0.817	
4c	2470.37	0.884	2472.50
	2471.70	0.664	
6	2470.81	0.187	2473.38
	2472.07	1.845	

[a] Derived from pseudo-Voigt deconvolution of the experimental spectrum. [b] Lowest energy edge transition derived from the peak maximum.

exhibit an additional low-energy pre-edge peak at 2470.21 and 2470.24 eV, respectively. This lower pre-edge feature at ~2470.2 eV has been assigned as a S 1s → 3p transition reflecting ligand π radical character (a ligand hole).[25−28,30−34] The intensity of this transition, defined by the area of the peak, is 0.9 units for **1b** and 1.3 units for **1a**. The latter suffers from photoreduction during the data collection that reduces the intensity of the first pre-edge peak away from the expected value of twice that for **1b**. As the neutral sample is scanned repeatedly for a period of a several hours, this peak diminishes until its intensity resembles that of the monoanion. Both **1a** and **1b** have a shoulder at 2471.08 and 2471.00 eV, respectively. These peaks are equivalent to the first pre-edge transition in **1c** at 2470.44 eV where the shift to lower energy is a result of having a fully reduced ligand set in the dianionic complexes. Therefore, we assign this low-energy transition as a ligand-based oxidation. Its intensity reflects the number of oxidative holes in the three dithiolene ligands of the dianions corresponding to 0, 1, and 2 holes in the dianion, monoanion and neutral, respectively. These results, in conjunction with the V K-edge energies, allow an unambiguous assignment of metal and ligand oxidation levels for the neutral species, the corresponding mono-, and dianions as noted in eq 1.

$$[V^{IV}(L_3{}^{4-})]^0 \underset{-e}{\overset{+e}{\rightleftharpoons}} [V^{IV}(L_3{}^{5-})]^{1-} \underset{-e}{\overset{+e}{\rightleftharpoons}} [V^{IV}(L_3{}^{6-})]^{2-} \quad (1)$$

These V K-edge and S K-edge measurements clearly establish that the redox processes are ligand-centered and that the central vanadium ion possesses a +IV oxidation state in all three cases.

Calculations. In this section, a picture of the electronic structures of complexes $[V(dithiolene)_3]^z$ ($z = 1+, 0, 1-, 2-, 3-, 4-$) and $[V(dtc)_3]^0$ is derived from broken symmetry (BS) DFT calculations by using the B3LYP functional for geometry optimizations and electronic properties. Although most of the compounds are anions, the use of the conductor-like screening model (COSMO)[64] had no effect on the computed geometry or electronic structure. The calculated geometries and metrical parameters of the [tris(dithiolene)vanadium]^z species were found to be in very good agreement with experimental values (where available). Typical of the B3LYP functional, the V−S bond lengths were overestimated by 0.05 Å. In particular, the geometry of the neutral forms, and of the monoanions, namely, $[V(pdt)_3]^{0/1-}$ and $[V(bdt)_3]^{1-}$, is trigonal prismatic, whereas that of the di-, tri-, and tetraanions is invariably distorted octahedral. The fold angle of the monoanions is clearly underestimated in the geometry optimized structures. These results are in very good agreement with experiment. Important calculated structural data are given in Table 9, where the two ligand types (L^A: pdt, mnt; L^B: bdt − *see* Scheme 3) and the full range of complex charges ($1+ \rightarrow 4-$) are represented. While the di-, tri- and tetraanions have structures ranging from distorted to near octahedral, and the monoanions have molecular C_{3h} symmetry, we will express their ground state electron configurations in D_{3h} symmetry for a simple comparison of this electron transfer series. A summary of the electronic structures across this series is displayed in Figure 8.

In general terms, these vanadium tris(dithiolene) complexes possess a 3-fold axis and therefore have the five vanadium d orbitals split into one nondegenerate a_1, the nonbonding d_{z^2} orbital, and two sets of degenerate e orbitals ($d_{x^2-y^2,xy}$ and $d_{xz,yz}$), that are π and σ bonding, respectively, with respect to three dithiolene ligands. These symmetry labels apply to molecules of D_3 symmetry, which is all species with twist angles not equal to 0° or 60°. For the latter, the structure and thus ligand field splitting is that of an octahedron; however, significant

Table 9. Mean Calculated Geometric Parameters of the $[V(pdt)_3]^z$ ($z = 1+, 0, 1-, 2-, 3-$), the $[V(mnt)_3]^z$ ($z = 1-, 2-, 3-, 4-$), and the $[V(bdt)_3]^z$ ($z = 1-, 2-, 3-$) Series Compared with Experimental Values Given in Parentheses

complex	S^a	z	V−S, Å	C−S, Å	C−C, Å	Θ°	α°
$[\mathbf{1a}]^+$	0	1+	2.333	1.717	1.405	32.1	0.8
1a	$^1/_2$	0	2.366	1.708	1.404	5.5	0.8
			(2.344)	(1.702)	(1.398)	(4.6)	(2.5)
1b	0	1−	2.384	1.728	1.388	0.8	12.8
			(2.334)	(1.731)	(1.374)	(0.8)	(23.7)
1c	$^1/_2$	2−	2.398	1.750	1.379	36.3	1.5
1d	1	3−	2.484	1.757	1.389	41.2	6.0
2b	0	1−	2.402	1.714	1.431	0.0	1.4
2c	$^1/_2$	2−	2.402	1.736	1.384	38.4	1.1
			(2.368)	(1.732)	(1.362)	(38.0)	(4.3)
2d	1	3−	2.491	1.743	1.391	42.3	6.1
2e	$^3/_2$	4−	2.631	1.745	1.403	45.7	1.0
3b	0	1−	2.397	1.731	1.423	0.5	13.5
			(2.350)	(1.739)	(1.411)	(1.3)	(22.6)
3c	$^1/_2$	2−	2.406	1.748	1.424	37.6	1.9
3d	1	3−	2.504	1.751	1.437	41.0	6.0

[a] Total spin ground state.

Scheme 3. Ligand Types

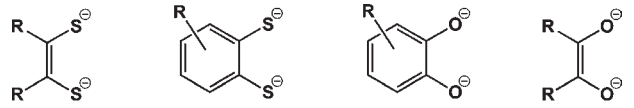

(64) Klamt, A.; Schuuramann, G. *J. Chem. Soc., Perkin Trans.* **1993**, *2*, 793.

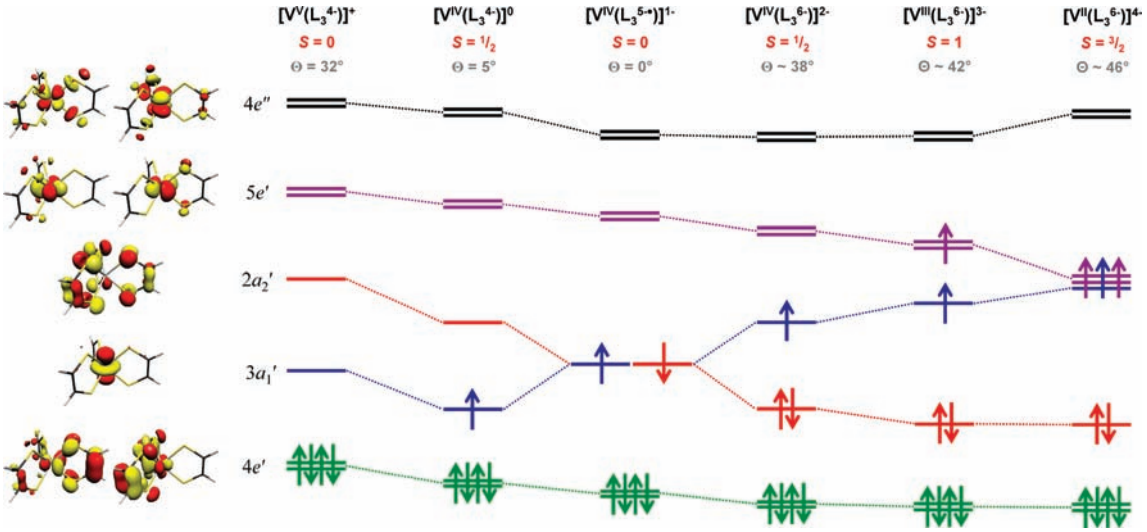

Figure 8. Qualitative MO scheme depicting the ordering of the frontier orbitals for the $[V(L_3)]^z$ ($z = 1+, 0, 1-, 2-, 3-, 4-$) electron transfer series derived from B3LYP DFT calculations. The MOs shown left are derived from the calculation of trigonal prismatic $[V(edt)_3]^0$ (**5a**) annotated with D_{3h} symmetry labels.

deviations from 60° arise because of the restrictions imposed by the ligand bite angle[65] that leads to a small splitting the essentially t_{2g} orbitals into *a* and *e* levels. Nevertheless, for simplicity, molecules with up to 25° deviations are still described as octahedral. For $\Theta = 0°$, the structure has a higher symmetry, that of D_{3h}, although the ligand field splitting is the same, with a_1', e', and e''. As can be seen in Figure 8, the splitting of the a_1' and e' orbitals decrease as the structure twists toward octahedral.

More interestingly, trigonal prismatic arrays of three dithiolene ligands act cooperatively. Individually, each dithiolate dianion is a 6π electron donor; there are four π orbitals, three of which are filled. When these are arranged in a trigonal prism, the highest occupied molecular orbital (HOMO) of each ligand forms one nondegenerate $2a_2'$ orbital that is non bonding with respect to the metal, and one degenerate e' orbital that is strongly π bonded to the metal d orbitals of like symmetry. Thus, oxidative holes are generated when electrons are removed from the a_2' orbital in these systems, and hence we characterize the three dithiolene ligand collectively as $(L_3)^{6-}$, with both the a_2' and e' level occupied; $(L_3)^{5-\bullet}$ where the a_2' is the singly occupied molecular orbital (SOMO) and thus the unpaired electron is shared by all three dithiolene ligands; and finally $(L_3)^{4-}$, in which the a_2' level is completely empty accounting for two holes but no unpaired electrons (radicals). This is an important distinction with octahedral tris(dithiolenes), such as the Cr electron transfer series,[26,27] and the thoroughly interrogated bis(dithiolene) complexes of late transition metals.[30,66,67] It is also worth considering that a further oxidation to $(L_3)^{3-\bullet}$ involves removal of a ligand electron from the e' state generating three oxidative holes though only one unpaired electron ($S_L = {}^1/_2$). The existence of this electron configuration in a trigonal prismatic array is highly unlikely, and as is described below, the ligands lose their interdependency, drift to an octahedral arrangement as $(L^{\bullet})_3$, $S_L = {}^3/_2$.

The key to defining the electronic structure of this vanadium tris(dithiolene) electron transfer series, or Mo, W, Re, for that matter, is the correct ordering of these predominately metal-based ($3a_1'$, $5e'$, $4e''$) and ligand-based ($2a_2'$, $4e'$) frontier orbitals.

Di-, Tri-, and Tetraanions. The spin-unrestricted B3LYP calculated electronic structures of the doublet state of the dianions $[V(pdt)_3]^{2-}$ (**1c**), $[V(mnt)_3]^{2-}$ (**2c**), and $[V(bdt)_3]^{2-}$ (**3c**) revealed in all cases the presence of a SOMO $(3a_1')^1$ in D_3 symmetry with ~86% V character. In addition, four empty metal-centered orbitals are identified as two sets of degenerate $5e'$ ($d_{x^2-y^2,xy}$) and $4e''$ ($d_{xz,yz}$) MOs—the hallmark of a V(IV) center in a trigonal ligand field. It should be noted that the $4e'$ MOs, the strong V−S π bonds, possess only 15% V d character, which is insufficient to describe the vanadium as a d^2 ion. The dithiolene ligands are identified as dithiolate(2−) species in all cases; the highest $2a_2'$ ligand-centered orbital is always doubly occupied. The electron configuration is $(4e')^4(2a_2')^2(3a_1')^1(5e')^0$ (Figure 8).

In the corresponding trianions, the metal-centered (~87% V) $5e'$ orbital is filled with a second unpaired electron (V(III); d^2; $S = 1$): $(4e')^4(2a_2')^2(3a_1')^1(5e')^1$. In tetraanionic $[V(mnt)_3]^{4-}$, the most reduced species experimentally observed, another electron enters this degenerate set of orbitals that is consistent with the interpretation of its IR spectrum. Thus, the V(II) d^3 central ion has a high-spin, $S = {}^3/_2$ ground state: $(4e')^4(2a_2')^2(3a_1')^1(5e')^2$, with three singly occupied orbitals of 88.3%, 91.0%, and 91.1% vanadium character, respectively, found in the spin-up manifold. This contrasts the isoelectronic Re(IV) analogue, which is d^3 $S = {}^1/_2$.[34] In both cases the three dithiolene ligands are closed-shell dithiolates-(2−), $(L_3)^{6-}$. Therefore, it is not surprising that the

(65) The magnitude of the twist angle Θ is a function of the bite angle of a bidentate ligand. The normalized bite angle is defined as the distance between the donor atoms of the chelate divided by the metal-ligand bond length (Kepert, D. L. *Prog. Inorg. Chem.* **1977**, *23*, 1). From this value, an octahedral limit (Θ_{lim}) can be determined for any given complex. Here, Θ_{lim} for aromatic dithiolates are typically smaller than for more flexible olefinic dithiolenes.

(66) Formitchev, D.; Lim, B. S.; Holm, R. H. *Inorg. Chem.* **2001**, *40*, 645.

(67) (a) Ray, K.; Weyhermüller, T.; Goossens, A.; Crajé, M. W.; Wieghardt, K. *Inorg. Chem.* **2003**, *42*, 4082. (b) Ray, K.; Weyhermüller, T.; Neese, F.; Wieghardt, K. *Inorg. Chem.* **2005**, *44*, 5345.

Table 10. Mulliken Spin Population Analysis from B3LYP DFT Ground State Calculations

complex	#[a]	ρ_V[b]	ρ_S[c]	ρ_C[d]
1a ($S = {}^1/_2$)	1	+1.375	−0.381	+0.009
1b ($S = 0$)	2	+1.478	−1.224	−0.220
1c ($S = {}^1/_2$)	1	+1.404	−0.456	+0.041
1d ($S = 1$)	2	+2.153	−0.231	+0.048
2b ($S = 0$)	2	+1.641	−1.456	−0.152
2c ($S = {}^1/_2$)	1	+1.431	−0.496	+0.064
2d ($S = 1$)	2	+2.156	−0.246	+0.085
2e ($S = {}^3/_2$)	3	+2.965	−0.159	+0.077
3b ($S = 0$)	2	+1.470	−1.249	−0.076
3c ($S = {}^1/_2$)	1	+1.355	−0.389	+0.048
3d ($S = 1$)	2	+2.157	−0.221	+0.044
6 ($S = 1$)	2	+2.157	−0.231	+0.046

[a] Total number of unpaired electrons ($\alpha + \beta$). [b] Vanadium spin density. [c] Total spin density on sulfur atoms. [d] Total spin density for the dithiolene (or dithiocarbamate) carbon atoms.

average calculated C−S bond length remains constant in each series of di-, tri-, and tetraanions whereas the average V−S distances increases with increasing negative charge.

The calculated Mulliken spin densities for the di-, tri-, and tetraanions show the presence of one, two, and three unpaired electrons at the vanadium ion, respectively (Table 10). A small amount of spin density is distributed over the six sulfur atoms because of polarization of the V−S π bonds of the 4e′ MOs: in **2c** there are 0.50 electrons distributed over six sulfur donor atoms, in trianionic **2d** there are 0.25, and in the tetraanion **2e** there are 0.16 electrons. The magnitude of the spin localized at the V is a function of the dithiolene ligand, with +1.404 for **1c**, +1.431 for **2c**, and +1.355 for **3c**. The highly electron withdrawing cyanide groups in $(mnt)^{2-}$ increase the polarization of the 4e′ MOs in **2c**, compared with **1c**, while the poorer π donating $(bdt)^{2-}$ ligand sees the least degree of spin polarization. Thus, the electron transfer series $[V(L)_3]^{2-,3-,4-}$ comprises three complexes containing three closed-shell dithiolate(2−) ligands, $(L_3)^{6-}$, and a V(IV) d^1 ($S = {}^1/_2$), V(III) d^2 ($S = 1$), V(II) d^3 ($S = {}^3/_2$) ion, respectively. In all cases the VS_6 polyhedron ranges from distorted octahedral to the octahedral limit for tris(dithiolene) complexes ($\Theta = 36.3-45.7°$).[65] It is meaningful to note that the same spin density distribution is seen for $[V^{III}(dtc)_3]$ (**6**) as in the calculated trianions in **1d**, **2d**, and **3d**. Neutral **6** possesses a genuine V(III) d^2 central ion confirmed experimentally. The calculated twist angle of 33.6° nicely replicates the crystallographic value of 32.0°.[68]

Diamagnetic Monoanions. The electronic structure of the singlet state monoanions $[V(pdt)_3]^{1-}$ (**1b**), $[V(mnt)_3]^{1-}$ (**2b**), and $[V(bdt)_3]^{1-}$ (**3b**) has been investigated using a broken symmetry BS(1,1) B3LYP method and, in addition, spin unrestricted $S = 0$ (singlet) and $S = 1$ (triplet) calculations. The former electronic structure may be interpreted as $[V^{IV}(L_3^{5-\bullet})]^{1-}$ where a V(IV) ion (d^1; $S_V = {}^1/_2$) is *antiferromagnetically* coupled to one ligand unpaired radical in the $(L_3)^{5-\bullet}$ ligand set ($S_L = {}^1/_2$) yielding an $S = 0$ ground state. The spin unrestricted singlet state is defined as $[V^V(L_3^{6-})]^{1-}$ with a diamagnetic V(V) center (d^0) and a diamagnetic $(L_3)^{6-}$ ligand set while the spin unrestricted triplet state ($S = 1$) is described as $[V^{IV}(L_3^{5-\bullet})]^{1-}$ where a V(IV) ion (d^1; $S_V = {}^1/_2$) is *ferromagnetically* coupled to one ligand unpaired radical $(L_3)^{5-\bullet}$ ($S_L = {}^1/_2$). While a triplet ground state may seem highly implausible in coordination complexes, it is possible in a trigonal prismatic geometry because the vanadium $3a_1'$ SOMO is orthogonal to the pure ligand $2a_2'$ SOMO. For **1b** and **3b**, the latter possibility can be excluded since they are diamagnetic for the full temperature range of 4−300 K.[69] Interestingly, both crystal structures exhibit prominent dithiolene chelate fold angles (av. $\alpha = 23.7°$ and 22.6°, respectively) that leads to a $D_{3h} \rightarrow C_{3h}$ symmetry reduction allowing the $3a_1'$ and $2a_2'$ orbitals to mix (as a').[32,34,70] Therefore, these orbitals can overlap which leads to the more favorable antiferromagnetically coupled ground state. For **2b**, the V K-edge data suggests this species is also trigonal prismatic; however, the degree of chelate fold, if any, cannot be ascertained without a crystal structure. However, a solid sample was shown to be diamagnetic at room temperature.[4] Nevertheless, to demonstrate the effectiveness and accuracy of our DFT calculations we have optimized geometries for all three possibilities ($S = 0$, $S = 1$, B(1,1) $S = 0$) for **2b** and **3b** (since these represent two dithiolene ligand types, L^A (mnt) and L^B (bdt) − *see* Scheme 3) starting with trigonal prismatic coordinates. The differences in the resultant structures are defined by their fold and twist angles, and compared using total energies. It is clearly apparent from the data in Table 11 that the BS(1,1) $S = 0$ solution is the most favorable, though only by ∼2 kcal mol^{-1} over the triplet and ∼3 kcal mol^{-1} over the singlet solutions, respectively, calculated using a spin unrestricted Kohn−Sham (UKS) method. Therefore, it is difficult to evaluate the correct electronic description based on the DFT calculations alone. All three structures are highly trigonal prismatic and but vary greatly in their chelate fold angle, which is non-existent for the $S = 1$ species to maintain orthogonal SOMOs and ∼25° for the UKS $S = 0$ species. The values for the BS(1,1) structures themselves are quite different, with 13.5° calculated for **3b**, which is a significant underestimate of the experimental value of 22.6°, and a meager 1.4° for **2b**.

From the large fold angle and negligible twist angle, the UKS computed $[V^V(L_3^{6-})]^{1-}$ ($S = 0$) structure appears to fit the crystallographic data. The large fold angle

Table 11. Relative Total Energies,[a] Average Twist and Fold Angles for the Geometry Optimized Structures Derived from UKS Singlet and Triplet, and BS(1,1) Singlet States

	state	α°	Θ°	relative total energy
2b	UKS, $S = 0$	24.4	0.2	+3.06
	UKS, $S = 1$	1.1	0.2	+2.31
	BS(1,1), $S = 0$	1.4	0.0	0.00
3b	UKS, $S = 0$	26.9	0.2	+2.91
	UKS, $S = 1$	0.8	0.2	+2.26
	BS(1,1), $S = 0$	13.5	0.5	0.00

[a] In kcal mol^{-1}. Lowest energy solution set to zero in each case.

(68) Zhu, H.-P.; Deng, Y.-H.; Huang, X.-Y.; Chen, C.-N.; Liu, Q.-T. *Acta Crystallogr.* **1997**, *C53*, 692.

(69) A significant amount of TIP (temperature independent paramagnetism) was used to simulate the magnetic data recorded for **3b**, which we suspect is the same cause for the "residual paramagnetism" seen in the magnetic data for $[NEt_4][V(pdt)_3]$, $[AsPh_4][V(mnt)_3]$, and $[AsPh_4][V(tfd)]$ (tfd = bis(trifluoromethyl)ethylenedithiolate) published in ref 4.

(70) Campbell, S.; Harris, S. *Inorg. Chem.* **1996**, *35*, 3285.

generates a V(V) d^0 central ion by virtue of the configurational interaction between the $3a_1'$ and $2a_2'$ that mix as a' in C_{3h} symmetry leading to a destabilized $3a_1'$ MO to the extent that it is empty. This situation is paralleled by a Fenske−Hall study of isoelectronic neutral molybdenum tris(dithiolenes), where the central ion is described as Mo(VI) d^0,[70] and contrasted by a recent combined experimental and theoretical study wherein the $3a_1'$ was the stabilized orbital through this interaction (implying Mo(IV) d^2).[32] However, both the V and S K-edge data explicitly rule out a V(V) oxidation state, instead clearly indicating V(IV) for all these vanadium tris(dithiolene) monoanions. And given the similarity of the electronic absorption spectra, we have concluded that a singlet diradical $[V^{IV}(L_3^{5-\bullet})]^{1-}$ ($S = 0$) is the correct electronic structure description for the monoanions in **1b**, **2b**, and **3b**, with the electron configuration $(4e')^4(3a_1')^1(2a_2')^1(5e')^0$ (Figure 8).

While the optimized twist angles are in excellent agreement with the experimental ones, the fold angles are routinely underestimated at 12.8° and 13.5° (crystallographically 23.7° and 22.6°, respectively) for **1b** and **3b**, respectively. It can be interpreted that the dithiolene fold increases the antiferromagnetic coupling between the two unpaired electrons, located in the $3a_1'$ and $2a_2'$ MOs. An orbital overlap integral $S_{ovlp} = 0.41$ is computed for **1b**, and represents the extent of spatial overlap of the two SOMOs.[49] A value of $S_{ovlp} = 0$ indicates the two magnetic orbitals are orthogonal, whereas $S_{ovlp} = 1$ implies a doubly occupied orbital (DOMO). For **3b**, $S_{ovlp} = 0.38$, while for **2b**, $S_{ovlp} = 0.04$, and implies that orbitals are nearly orthogonal and consistent with the small calculated twist angle of 1.4°. The exchange coupling constant, determined from the high-spin and BS energies together with the corresponding spin-expectation values $\langle S^2 \rangle$ according to the Yamaguchi approach (eq 2),[71] is calculated to be -3119 cm^{-1} and -3068 cm^{-1} for **1b** and **3b**, respectively, which is in keeping with the absence of any paramagnetism over the temperature range of 4−300 K. The calculated value of $J = -925$ cm^{-1} for **2b** is considerably lower, though there was no report of any magnetic behavior at room temperature.[4,69]

$$J = \frac{E_{HS} - E_{BS}}{\langle S^2 \rangle_{HS} - \langle S^2 \rangle_{BS}} \qquad (2)$$

The results from a Mulliken spin population analysis of the monoanions **1b**, **2b**, and **3b** are listed in Table 10. In each case, more than one unpaired electron is located at the vanadium (α-spin) and ligands (β-spin) because of the aforementioned spin polarization of the $4e'$ MOs. The polarization is greater for these monoanions than the corresponding dianions since the energetic separation of the occupied $4e'$, $3a_1'$, and $2a_2'$ MOs is much smaller.

Doublet Neutral Species. The calculated structure of the neutral species $[V(pdt)_3]$ (**1a**) with an $S = {}^1/_2$ ground state has been calculated using spin-unrestricted Kohn−Sham (UKS) DFT methodology (B3LYP functional).

(71) (a) Soda, T.; Kitagawa, Y.; Onishi, T.; Takano, Y.; Shigetu, Y.; Nagao, H.; Yoshioka, Y.; Yamaguchi, K. *Chem. Phys. Lett.* **2000**, *319*, 223. (b) Yamaguchi, K.; Takahara, Y.; Fueno, T. In *Applied Quantum Chemistry*; Smith, V. H., Ed.; Reidel: Dordrecht, The Netherlands, 1986; p 155.

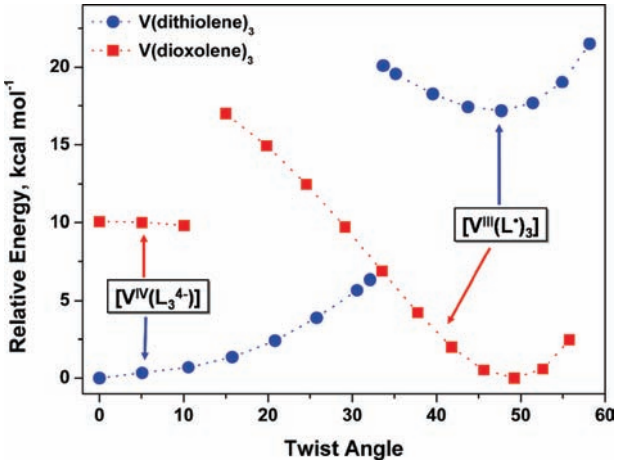

Figure 9. Walsh-type plot of the total electronic energies of $[V(edt)_3]$ (**5a**) (filled blue circles) and $[V(cat)_3]$ (filled red squares) as a function of the trigonal twist angle (Θ), derived from spin-restricted BS(3,2) single point DFT calculations. In each case, the lowest energy solution has been set to zero.

Importantly, no BS solution could be found. The VS_6 polyhedron is trigonal prismatic (av. Θ = 5.5°) and the unpaired electron was found to reside in a vanadium-centered d_{z^2} orbital (86% V character), namely, $3a_1'$ in D_{3h} symmetry; there are four empty d orbitals ($5e'$ and $4e''$) which indicates a +IV (d^1, $S = {}^1/_2$) oxidation state of the vanadium ion and a $(4e')^4(3a_1')^1(2a_2')^0(5e')^0$ electron configuration for the complex. The fully occupied degenerate $(4e')^4$ MOs indicate the presence of a diamagnetic $(L_3)^{4-}$ ligand set. The three bidentate ligands accommodate two oxidative holes in the empty $2a_2'$ ligand orbital (which is the LUMO of the neutral species) as compared to three dithiolate(2−) ligands in $(L_3)^{6-}$; see Figure 8. The calculated short C−S distance at 1.708 Å and long C−C distance at 1.404 Å are in excellent agreement with the experimental values of 1.702(1) Å and 1.399(2) Å, respectively, for **1a** (Table 9). These values clearly indicate a $(L_3)^{4-}$ ligand set. The near identical vanadium spin population in **1a** and **1c** is the key reason for why their isotropic hyperfine values are strikingly similar.

We explored the potential energy surface as a function of the twist angle; single point calculations on fixed geometries were performed with neutral $[V^{IV}(edt)_3]$ (**5a**) for twist angles ranging from 0° to 60° (at 5° increments). The results are plotted in Figure 9, with the energy of the D_{3h} structure set to 0. Clearly, the trigonal prismatic solution is the most energetically favorable. There is an abrupt jump in the plot at Θ ∼ 31° to a second energy surface that possesses a minimum at Θ = 47.7°. This minimum sits 17.2 kcal mol^{-1} higher in energy than the trigonal prismatic structure and has an electronic structure described as $[V^{III}(L_3^{3-})]^0$ (or alternatively $[V^{III}(L^{\bullet})_3]^0$) where $(L_3)^{3-}$ represents three monoanionic dithiolene radical ligands, $S_L = {}^3/_2$. Here, the doublet spin state stems from antiferromagnetic coupling between the two unpaired electrons on the V(III) (d^2; $S_V = 1$) ion with two of the three ligand radicals ($S_L = {}^3/_2$). The same result was computed for the neutral Cr analogue, $[Cr^{III}(L^{\bullet})_3]^0$ where the opposite situation occurs: The octahedral structure is 20 kcal mol^{-1} more favorable than the trigonal prismatic $[Cr^{IV}(L_3^{4-})]$ solution.[26] By placing

the vanadium last on the atom list of the input file, a BS(3,2) geometry optimized structure was generated because when the symmetry was broken, the spin up (α-spin) electrons were localized on the ligands, whereas the spin down (β-spin) electrons were retained by the metal. This way, a broken symmetry solution was obtained, and in keeping with three oxidized holes on the tris(dithiolene) ligand set, the complex is distorted octahedral with Θ = 38.3°. Most interestingly, this species is 16.9 kcal mol^{-1} less favorable than the trigonal prismatic solution, and very close to the value obtained above (17.2 kcal mol^{-1}) for the static structures. Perhaps most intriguing is the difference in the plot of total energy as a function of the twist angle for the neutral vanadium tris(catecholate) analogue also traced in Figure 9. This exemplifies the stark difference between bidentate *O*,*O*′- and *S*,*S*′-donor bidentate ligands, as disclosed in the Discussion section below.

Diamagnetic Monocation. We have also calculated the molecular and electronic structure of the supposedly diamagnetic monocation $[V(pdt)_3]^{1+}$, $[\mathbf{1a}]^+$. We have not found a reasonable BS(1,1) solution for the $S = 0$ ground state. The spin unrestricted Kohn−Sham solution ($S = 0$) is stable yielding a distorted octahedral VS_6 polyhedron (Θ = 32.1°). The short C−S average distance at 1.717 Å indicates the presence of two ligand-based oxidative holes since these data are nearly identical with those found for the neutral species **1a**, $[V^{IV}(L_3{}^{4-})]^0$ (Table 9). The oxidation of the neutral species by one electron is then a metal-centered process generating a vanadium(V) ion (d^0): $[V^{V}(L_3{}^{4-})]^{1+}$ ($S = 0$). The calculated average V−S distance in the monocation is slightly shorter by 0.03 Å than in the corresponding neutral species.

Time-Dependent DFT Calculations. V K-Pre-Edge XAS. In the current study of vanadium tris(dithiolenes), it is necessary to corroborate our DFT-derived electronic structures by calculating experimental observables. To this end, we have used a simple time-dependent DFT (TD-DFT) method[51,52] for simulating the pre-edge features seen in the vanadium and sulfur K-edge spectra. Such an approach has been very successful in calculating the metal and sulfur K-edges of tris(dithiolene) complexes of Cr and Mn,[26] and Re.[34] For this system, there is a profound difference in the electronic structure for the vanadium tris(dithiolene) monoanion calculated by the BP86 and B3LYP functionals, namely, the former gives no broken symmetry solution, hence the latter functional is utilized despite the more lengthy computation time. Additionally, because of the limitations in the accurate treatment of excited states in DFT, *absolute* transition energies cannot be obtained by this method. Nevertheless, the *relative* transition energies and the *relative* intensities are, in general, reliably modeled. For a given theoretical method, that is, combination of functional, basis sets, relativistic treatment, and so forth, an empirical correction for the energy and intensity can be introduced. For the present study, the calculated V K-edge spectra are shifted by +116.3 eV and are depicted with a 1 eV broadening. The calculated V K-pre-edge spectra for **1a**, **1b**, **2c** and **6** are shown in Figure 10; the data are summarized in Table 12.

An excellent fit is afforded by the calculated V K-pre-edge spectra in both the relative energy and the intensity

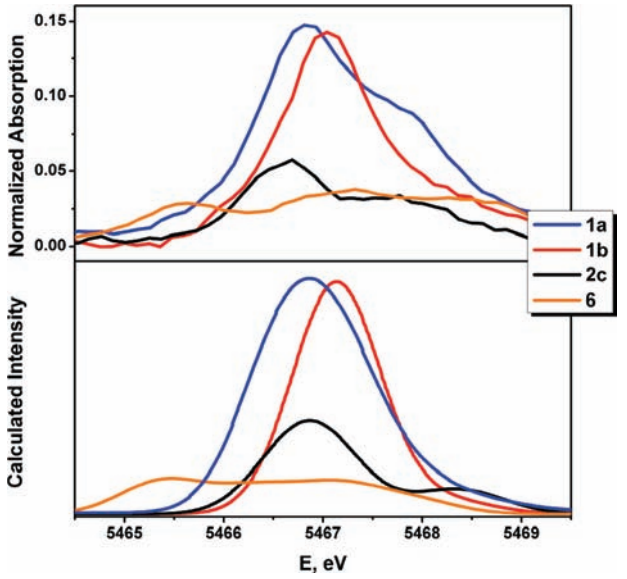

Figure 10. Experimental (top) and calculated (bottom) V K-pre-edge spectra for **1a** (blue), **1b** (red), **2c** (black), and **6** (orange) obtained from B3LYP TD-DFT calculations. Calculated intensity in arbitrary units.

Table 12. Calculated and Experimental V K-Pre-Edge Transition Energies

		transition energies[b]	
complex	transition[a]	calculated[c]	experimental
1a	1s → 5*e*′	5466.9	5466.9
		5467.9(sh)	5467.6
1b	1s → 5*e*′	5467.1	5467.0
2b	1s → 5*e*′	5467.2	5467.2
2c	1s → 5*e*′	5466.9	5466.7
	1s → 4*e*″	5468.3	5467.8
4c	1s → 5*e*′	5466.8	5466.7
		5468.4	5467.9
6	1s → 5*e*′(α)	5465.5	5465.7
	1s → 5*e*′(β)	5467.1	5467.4

[a] Largest contribution to calculated pre-edge peak. [b] In eV. [c] Shifted by +116.3 eV.

of the experimental pre-edge region. For the monoanion in **1b**, one peak is observed, whereas two peaks are accounted for in the spectrum of **2c** and neutral **6**. However, the shoulder seen experimentally in the spectrum of **1a** is not reproduced; instead a very broad pre-edge peak is derived from the computation. Nonetheless, the relative energies are found within 0.2 eV of the experimental values. The first pre-edge feature in the spectrum of **6**, containing a genuine V(III) central ion, is calculated to be 1.4 eV lower in energy than the corresponding feature for **1a**, which is similar to the experimentally observed difference of 1.2 eV.

The intensity of the pre-edge peaks is determined by the extent of V 3d−4p mixing in the frontier orbitals. Figure 11 depicts the individual transitions and their intensities as a sum of dipole-allowed and quadrupole-allowed components for neutral $[V(pdt)_3]$ (**1a**). The calculations reveal that the pre-edge intensity for **1a** and **1b** is dominated by transitions to the vacant 5*e*′ MOs; their trigonal prismatic geometry generates ∼4% V 4p character in these orbitals (Table 13). The broadening of the peak, in the range of 1.1 eV, stems from the spin polarization of the unoccupied orbitals; the polarization of the 5*e*′ level is

0.6 eV for **1a** and 0.4 eV in **1b**, giving a much broader simulation for the former. There are contributions to this prominent peak from transitions to the vacant $3a_1'(\beta)$ MO, though these are almost negligible since it bears no V 4p character. At higher energies, a tail is seen in the simulation because of contributions from 1s → $4e''$ transitions. These orbitals are predominantly metal-centered and possess miniscule 4p character; hence, no dipole character contributions are observed for these transitions (Figure 11). The notable intensity of the experimental shoulder at 5467.6 eV in **1a** is difficult to account for based on this approach and may stem from an underestimation of the polarization of the unoccupied orbitals. Both **1a** and **5a** exhibit this feature.

In D_{3h} and C_{3h} point symmetry, there is also no 4p contribution to the unoccupied $4e''$, so transitions to these MOs have low intensity and lead to a sloping of the pre-edge peak in **1b** at higher energies. The experimental line width of ~1 eV is also nicely matched by the calculation; the broadening generated by polarization of the $5e'$ MOs by almost 0.4 eV. More importantly, the calculated pre-edge spectrum for **2b** closely replicates the experimental spectrum (Supporting Information, Figure S45). This validates the assignment of its electronic and geometric structure as trigonal prismatic $[V^{IV}(L_3^{5-\bullet})]^{1-}$ ($S = 0$) in the absence of a crystal structure.

The first pre-edge peak in the spectra of **2c** (Figure 10) and **4c** (Supporting Information, Figure S46) is the same as that described above for **1a** and **1b**. The intensity is diminished since the trigonal twist angle is considerably higher toward a distorted octahedral geometry that halves the V 4p content of the $5e'$ MOs. However, this twist introduces 4p character into the $4e''$ MOs since they now comprise an admixture of $d_{xz,yz}$ and $d_{x^2-y^2,xy}$; the latter d orbitals carry p contributions. This generates a second pre-edge peak in the spectra of dianions **2c** and **4c** that occurs at roughly the same energy as the analogous transition in **1a** and **1b** but with greater intensity. The calculations overestimate the ligand field splitting (separation of the $5e'$ and $4e''$ levels) by 0.4 eV for both **2c** and **4c**. The line broadening is a result of spin polarization of the $5e'$ MOs that is of the same magnitude (~0.4 eV) as for the neutral and monoanionic complexes of this series. For **6**, the first pre-edge peak is assigned to the 1s → $5e'(\alpha)$ level, which is half occupied and thus the peak is less intense than the corresponding transition in **2c** (and **4c**). The high-spin V(III) d^2 configuration leads to a very large 1.1 eV splitting of the $5e'(\alpha)$ and $5e'(\beta)$ states, and the second pre-edge peak is dominated by β-spin transitions to the $5e'$ level. Thus, the two pre-edge transitions in **6** are equivalent to the first pre-edge transition in **1a**, **1b**, and **2c**. When summed, the intensity of the first two peaks in **6** is approximately equal to the first peak in **2c** (and **4c**) despite its d^2 configuration. This stems from the reduced bite angle of the $(dtc)^{1-}$ ligand that inhibits the degree of trigonal twisting toward an octahedral structure ($\Theta_{calcd} = 33.6°$), and therefore more V 4p character is retained in the $5e'$ MOs in **6** (Table 13). Furthermore, the 1s → $4e''$ transitions contribute to the second pre-edge feature occurring 1.3 eV lower than the same transition for the V(IV) species.

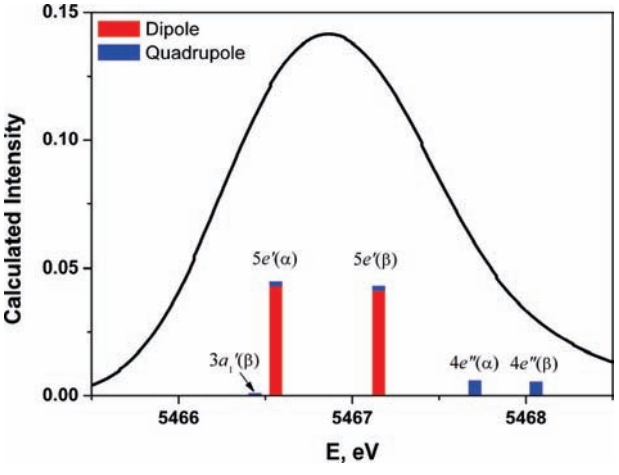

Figure 11. Simulated V K-pre-edge spectrum of **1a** (black) and stick plot showing the dipole (red) and quadrupole (blue) contributions to the pre-edge transitions. The total calculated intensity is the sum of these components in arbitrary units.

S K-Pre-Edge XAS. The experimental and calculated S K-pre-edge XAS spectra for the $[V(pdt)_3]^{0/1-/2-}$ electron transfer series are compared in Figure 12, with the peak energies listed in Table 14. The simulated spectra present a very reasonable fit of the experimental data, with the first pre-edge peak for all three compounds calculated within 0.2 eV of the experiment. For neutral **1a** and monoanionic **1b**, three pre-edge peaks arise. The first is identified at the 1s → $2a_2'$ transition, which is unoccupied in **1a** and singly occupied in **1b**. The calculated intensity ratio is 1.77:1.00 (**1a**/**1b**), not far off the experimental (1.45:1.00) ratio because of the aforementioned photoreduction of **1a** that reduces the peak intensity. The sulfur 3p character in this orbital is estimated at 62.1% (**1a**) and 64.0% (**1b**), respectively (Supporting Information, Table S46). The experimental line width (fwhm) of ~0.84 eV is consistent with a single transition. The second transition is manifested as a shoulder in the experimental data, and is described as 1s → $5e'(\alpha)$ transition. Here, spin polarization of the $5e'$ MOs is estimated at ~0.4 eV, so the

Table 13. Vanadium 3d and 4p Contributions (%) to the Lowest Unoccupied MOs Derived from B3LYP DFT Calculations

	1a		**1b**		**2b**		**2c**		**4c**		**6**	
	3d	4p	3d	4p	3d	4p	3d	4p	3d	4p	3d	4p
$3a_1'(\beta)$	56.8	0.0	47.4	0.0	58.3	0.0	37.3	0.0	59.8	0.2	73.9	0.0
$5e'(\alpha)$	57.3	2.0	54.1	2.0	53.9	1.7	54.5	1.1	59.7	1.2	72.1	1.3
	56.3	2.0	54.8	1.9	54.9	1.7	54.8	1.0	62.1	1.0		
$5e'(\beta)$	64.7	2.1	67.1	2.2	72.3	2.2	71.7	1.0	64.0	0.8	56.4	1.3
	64.4	2.1	64.3	2.2	72.0	2.2	72.1	0.9	65.6	0.8	47.7	2.0
$4e''(\alpha)$	47.1	0.0	50.3	0.0	45.2	0.0	52.1	0.1	34.2	0.2	59.5	0.1
	50.9	0.0	50.0	0.0	45.1	0.0	51.7	0.1	47.9	0.2	49.0	0.5
$4e''(\beta)$	56.2	0.1	50.2	0.2	58.0	0.0	52.7	0.2	48.8	0.1	67.1	0.0
	55.7	0.1	48.4	0.5	57.7	0.0	52.9	0.2	39.6	0.1	64.1	0.0

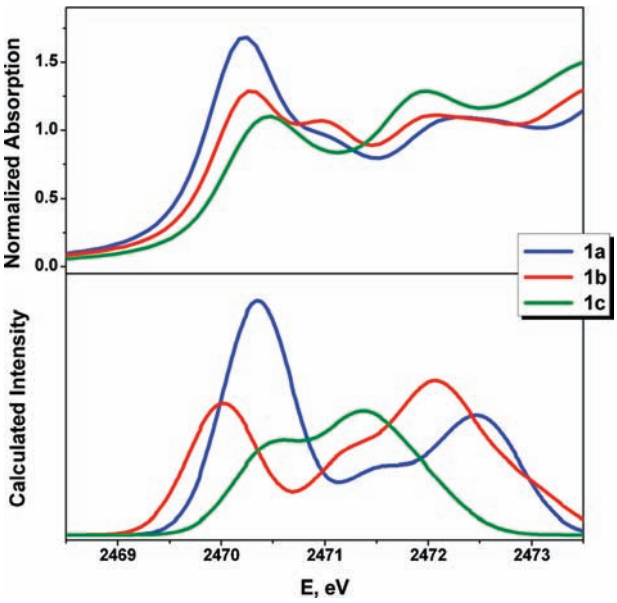

Figure 12. Experimental (top) and calculated (bottom) S K-pre-edge spectra for **1a** (blue), **1b** (red), and **1c** (green) obtained from B3LYP TD-DFT calculations. Calculated intensity in arbitrary units.

Table 14. Calculated and Experimental S K-Pre-Edge Transition Energies

		transition energies[a]	
complex	transition	calculated[b]	experimental
1a	$1s \rightarrow 2a_2'$	2470.35	2470.21
	$1s \rightarrow 5e'(\alpha)$	2471.66	2471.08
		2472.46	2472.04
1b	$1s \rightarrow 2a_2'$	2470.02	2470.24
	$1s \rightarrow 5e'(\alpha)$	2471.29	2471.00
		2472.07	2471.98
1c	$1s \rightarrow 5e'(\alpha)$	2470.61	2470.44
		2471.37	2471.92
2c	$1s \rightarrow 5e'(\alpha)$	2470.37	2470.54
		2471.55	2471.47
3c	$1s \rightarrow 5e'(\alpha)$	2470.37	2470.36
		2471.07	2471.77
4c	$1s \rightarrow 5e'(\alpha)$	2470.37	2470.37
		2471.09	2471.70
6	$1s \rightarrow 5e'(\alpha)$	2470.72	2470.81
	$1s \rightarrow 5e'(\beta)$[c]	2471.86	2472.07

[a] In eV. [b] Shifted by +57.41 eV. [c] Significant contributions from $1s \rightarrow$ dtc π^* transitions.

corresponding $1s \rightarrow 5e'(\beta)$ transition contributes to the calculated peak at 2472.46 and 2472.07 eV, respectively. The intensity of this transition is the same in both **1a** and **1b** (1.04:1.00) because of the similar S 3p contribution in the $5e'(\alpha)$ MOs (Supporting Information, Table S46); the peak is calculated to be 0.4 eV higher in energy for **1a** because of the more oxidized ligand set in this complex. The TD-DFT also suggests a small contribution for transitions to the vacant $3a_1'(\beta)$ state with $< 10\%$ S 3p character, although the experimental line width is the same as the first pre-edge feature, implying a negligible contribution from this excitation. The third calculated peak is a composite of several transitions to low-lying C−S π^*, $4e''$, and the $5e'(\beta)$ orbitals. The large experimental line width (1−1.2 eV) attests to the multiple transitions generating this feature.

Two pre-edge transitions are calculated for the dianion in **1c**, at 2470.61 and 2471.37 eV, respectively. The latter is a 0.6 eV underestimate of the corresponding peak in the experimental spectrum; nonetheless, the large line width indicates several transitions contributing to this feature. The first pre-edge peak is defined as predominately $1s \rightarrow 5e'(\alpha)$; however, the difference in the experimental and calculated line width is quite pronounced. The dianions in **2c**, **3c**, and **4c** have a similar discrepancy between the experimental and calculated first pre-edge feature (Supporting Information, Figure S24, bottom). For the aromatic-1,2-dithiolate derivatives, three peaks are calculated, with the second assigned to the $1s \rightarrow 5e'(\alpha)$ transition only. This suggests an overestimation of the polarization of the $5e'$ MOs in these calculations.

In the simulation of **6**, the TD-DFT calculations nicely reproduce the small pre-edge shoulder (at 2470.72 eV; Supporting Information, Figure S25, bottom) seen in the experiment (2470.81 eV). Its intensity is significantly weaker than the corresponding transition in the spectra of the dianions (**1c**, **2c**, **3c**, **4c**; Supporting Information, Figure S24, bottom) because there is only one hole in the $5e'(\alpha)$ orbitals in this V(III) d^2 complex and the calculated sulfur 3p content of 7.5% overall gives rise to this faint pre-edge feature. The second peak is again a collection of transitions to the $5e'(\beta)$ and low-lying C−S π^* orbitals of the $(dtc)^{1-}$ ligand.

Discussion

In this section we will attempt to establish the factors which govern the molecular (trigonal prismatic versus octahedral MS_6 or MO_6 polyhedra) and electronic structures of each member of the electron transfer series of tris(dithiolene) metal or tris(dioxolene) metal complexes where L^A, L^B, L^D, and L^E have formulae defined in Scheme 3. A summary is provided in Table 15.

It has been shown electrochemically that the four-membered series $[Cr^{III}(L^A)_3]^z$, $[Cr^{III}(L^B)_3]^z$, and $[Cr^{III}(L^D)_3]^z$ (z = 0, 1−, 2−, 3−)[26,27,72−74] exist. All redox processes are ligand-centered (Table 15); each complex invariably contains a central Cr(III) ion (d^3, $S_{Cr} = {}^3/_2$, $t_{2g}{}^3$). The structure of the CrS_6 or CrO_6 polyhedron is distorted octahedral in all cases. The neutral species possess a singlet ground state ($S = 0$) composed of a central Cr^{III} ion where the three unpaired $t_{2g}{}^3$ electrons are coupled intramolecularly antiferromagnetically to three π radical monoanions $(L^A)^{1-\bullet}$, $(L^B)^{1-\bullet}$, $(L^D)^{1-\bullet}$, $(L^E)^{1-\bullet}$: $[Cr^{III}(L^{A,B,D,E\bullet})_3]^0$ ($S = 0$).[26,27,75]

In contrast, the octahedral trianions, $[Cr^{III}(L^{A,B,D})_3]^{3-}$, contain a central Cr(III) ion and three fully reduced diamagnetic dithiolate(2−) or catecholate(2−) ligands. They possess an $S = {}^3/_2$ ($t_{2g}{}^3$) ground state and represent classical Werner-type coordination compounds. The paramagnetic monoanions ($S = {}^1/_2$) and dianions ($S = 1$) contain two and one π radical monoanion, respectively, and a central Cr(III) ion.

(72) (a) Buchanan, R. M.; Clafin, J.; Pierpont, C. G. *Inorg. Chem.* **1983**, *22*, 2552. (b) Isied, S. S.; Kuo, G.; Raymond, K. N. *J. Am. Chem. Soc.* **1976**, *98*, 1763. (c) Pierpont, C. G. *Coord. Chem. Rev.* **2001**, *216−217*, 99. (d) Pierpont, C. G. *Coord. Chem. Rev.* **2001**, *219−221*, 415. (e) Pierpont, C. G.; Buchanan, R. M. *Coord. Chem. Rev.* **1981**, *38*, 45. (f) Pierpont, C. G.; Lange, C. W. *Prog. Inorg. Chem.* **1994**, *41*, 331.

(73) (a) Pierpont, C. G.; Downs, H. H. *J. Am. Chem. Soc.* **1976**, *98*, 4834. (b) Sofen, S. R.; Ware, D. C.; Cooper, S. R.; Raymond, K. N. *Inorg. Chem.* **1979**, *18*, 234.

(74) Raymond, K. N.; Isied, S. S.; Brown, L. D.; Fronczek, F. R.; Nibert, J. H. *J. Am. Chem. Soc.* **1976**, *98*, 1767.

(75) Spikes, G. H.; Sproules, S.; Bill, E.; Weyhermüller, T.; Wieghardt, K. *Inorg. Chem.* **2008**, *48*, 10935.

Table 15. Molecular and Electronic Structures of $[M(L)_3]^z$ Complexes (M = V, Cr, Mo, Re; $L^{A,B}$ = dithiolene; L^D = dioxolene)[a]

dithiolene				dioxolene			
compound	S[b]	geometry[c]	ref	compound	S[b]	geometry[c]	ref
$[V^V(L^{A,B\bullet})_2(L^{A,B})]^{1+d}$	0	dist. oct.[e]	this work	$[V^V(L^{D\bullet})(L^D)_2]^0$ or			
$[V^{IV}(L^{A,B\bullet})_2(L^{A,B})]^{0d}$	$^1/_2$	t.p.	this work[f]	$[V^{III}(L^{D\bullet})_3]^{0g}$	$^1/_2$	oct.	77
$[V^{IV}(L^{A,B\bullet})(L^{A,B})_2]^{1-h}$	0	t.p.	this work[f]	$[V^V(L^D)_3]^{1-}$	0	oct.	78
$[V^{IV}(L^{A,B})_3]^{2-}$	$^1/_2$	dist. oct.	this work[f]	$[V^{IV}(L^{D,E})_3]^{2-}$	$^1/_2$	oct/t.p.	75,79−82
$[V^{III}(L^{A,B})_3]^{3-}$	1	oct.[e]	this work	$[V^{III}(L^D)_3]^{3-}$	1	oct.	79,83
$[V^{II}(L^{A,B})_3]^{4-}$	$^3/_2$	oct.[e]	this work				
$[Cr^{III}(L^{A,B\bullet})_3]^{0g}$	0	oct. [e]	26, 27	$[Cr^{III}(L^{D,E\bullet})_3]^0$	0	oct.	27,73,75,76
$[Cr^{III}(L^{A,B\bullet})_2(L^{A,B})]^{1-g}$	$^1/_2$	oct.	27	$[Cr^{III}(L^{D\bullet})_2(L_D)]^{1-g}$	$^1/_2$	oct.	76,84
$[Cr^{III}(L^{A,B\bullet})(L^{A,B})_2]^{2-g}$	1	oct.	26,85	$[Cr^{III}(L^{D\bullet})(L^D)_2]^{2-g}$	1	oct.	76,84
$[Cr^{III}(L^{A,B})_3]^{3-}$	$^3/_2$	oct.	85	$[Cr^{III}(L^D)_3]^{3-}$	$^3/_2$	oct.	74
$[Mo^{IV}(L^{A\bullet})_2(L^A)]^{0d}$	0	t.p.	86,87	$[Mo^{VI}(L^D)_3]^0$	0	t.p.	88
$[Mo^{IV}(L^{A\bullet})(L^A)_2]^{1-h}$	$^1/_2$	t.p./dist. oct.	87	$[Mo^V(L^D)_3]^{1-}$	$^1/_2$	unknown	
$[Mo^{IV}(L^A)_3]^{2-}$	0	t.p./dist. oct.	66,89	$[Mo^{IV}(L^D)_3]^{2-}$	0	unknonn	
$[Mo^V(L^{B\bullet})(L^B)_2]^{0h}$ or							
$[Mo^{IV}(L^{B\bullet})_2(L^B)]^{0d}$	0	t.p.	28,90				
$[Mo^V(L^B)_3]^{1-}$	$^1/_2$	t.p./dist. oct.	28,91,92				
$[Mo^{IV}(L^B)_3]^{2-}$	0	t.p./dist. oct.	92−94				
$[Re^V(L^{A,B\bullet})_2(L^{A,B})]^{1+d}$	0	t.p.[e]	34	$[Re^{VII}(L^D)_3]^{1+}$ or			
$[Re^V(L^{A,B\bullet})(L^{A,B})_2]^{0h}$	$^1/_2$	t.p.	95	$[Re^{VI}(L^{D\bullet})(L^D)_2]^{1+g}$	0	unknown	
$[Re^V(L^{A,B})_3]^{1-}$	0	t.p./dist t.p.	34	$[Re^{VI}(L^D)_3]^0$	$^1/_2$	oct.	96,97
$[Re^{IV}(L^{A,B})_3]^{2-}$	$^1/_2$	oct.	98	$[Re^V(L^D)_3]^{1-}$	0	unknown	
$[Re^{III}(L^{A,B})_3]^{3-}$	1	oct.[e]	34	$[Re^{IV}(L^D)_3]^{2-}$	$^1/_2$	unknown	
$[Re^{II}(L^{A,B})_3]^{4-}$	$^3/_2$	oct.[e]	34				

[a] Abbreviations: t.p. = trigonal prismatic. oct. = octahedral. dist. = distorted. Ligand formulae defined in Scheme 3. [b] Total spin ground state. [c] Geometry determined by X-ray crystallography or theoretical optimization. [d] The two oxidative ligand holes are delocalized over all three ligands (L_3^{4-}), $S_L = 0$. [e] Determined by geometry optimization. [f] Refer to Table 1 for relevant references. [g] The ($L^{1-\bullet}$) π radical is localized (class I or II). [h] The oxidative ligand hole is delocalized over all three ligands $(L_3)^{5-\bullet}$, $S_L = {}^1/_2$.

These complexes display ligand-to-ligand intervalence charge transfer bands >1000 nm ($\varepsilon \approx 10^4$ M^{-1} cm^{-1}) that may involve class II ligand mixed valency.[26,27,76]

The series $[Re(L^B)_3]^z$ ($z = 1+, 0, 1-, 2-, 3-$) has recently been investigated (Table 15).[34] It has been established that the diamagnetic monoanion contains a distorted trigonal prismatic ReS_6 polyhedron with a central Re(V) ion (d^2, $S = 0$) and three diamagnetic benzene-1,2-dithiolate(2−) ligands. The di- and trianions, ($S = {}^1/_2$) and ($S = 1$), respectively, contain a Re(IV) and a Re(III) ion in an octahedral environment of three closed-shell dithiolate ligands. Interestingly, the neutral and monocationic species contain one and two ligand-centered, oxidative holes, respectively, which are delocalized over all three ligands. Their ReS_6 core structures are trigonal prismatic.[34,95] The corresponding oxygen containing di- and monoanionic complexes $[Re(DBCat)_3]^{2-/1-}$ (DBCat = 3,5-di-*tert*-butylcatecholate) contain both three diamagnetic catecholate(2−) ligands and a central Re^{IV} (d^3; $S = {}^1/_2$) and a Re^V (d^2; $S = 0$) ion, respectively.[96,99] It is now very important to note that neutral $[Re(L^D)_3]$ complexes possess a doublet ground state and an octahedral ReO_6 polyhedron.[96,99] The electronic structures of trigonal prismatic $[Re^V(L^{A,B\bullet})(L^{A,B})_2]^0$ and of octahedral $[Re^{VI}(L^D)_3]^0$ are clearly different. In the former the unpaired electron is delocalized

(76) Chang, H.-C.; Myasaka, H.; Kitagawa, S. *Inorg. Chem.* **2001**, *40*, 146.
(77) Morris, A. M.; Pierpont, C. G.; Finke, R. G. *Inorg. Chem.* **2009**, *48*, 3496.
(78) (a) Cass, M. E.; Gordon, N. R.; Pierpont, C. G. *Inorg. Chem.* **1986**, *25*, 3962. (b) Yin, C.-X.; Finke, R. G. *J. Am. Chem. Soc.* **2005**, *127*, 9003.
(79) Cooper, S. R.; Koh, Y. B.; Raymond, K. N. *J. Am. Chem. Soc.* **1982**, *104*, 5092.
(80) (a) Hou, Z.; Stack, T. D. P.; Sunderland, C. J.; Raymond, K. N. *Inorg. Chim. Acta* **1997**, *263*, 341. (b) Karpishin, T. B.; Dewey, T. M.; Raymond, K. N. *J. Am. Chem. Soc.* **1993**, *115*, 1842. (c) Karpishin, T. B.; Raymond, K. N. *Angew. Chem., Int. Ed. Engl.* **1992**, *31*, 466.
(81) Karpishin, T. B.; Stack, T. D. P.; Raymond, K. N. *J. Am. Chem. Soc.* **1993**, *115*, 182.
(82) Milsmann, C.; Levina, A.; Harris, H. H.; Foran, G. J.; Turner, P.; Lay, P. A. *Inorg. Chem.* **2006**, *45*, 4743.
(83) Bulls, A. R.; Pippin, C. G.; Hahn, F. E.; Raymond, K. N. *J. Am. Chem. Soc.* **1990**, *112*, 2627.
(84) (a) Chang, H.-C.; Ishii, T.; Kondo, M.; Kitagawa, S. *J. Chem. Soc., Dalton Trans.* **1999**, 2467. (b) Chang, H.-C.; Kitagawa, S. *Angew. Chem., Int. Ed.* **2002**, *41*, 130.
(85) Lewis, G. R.; Dance, I. *J. Chem. Soc., Dalton Trans.* **2000**, 3176.
(86) (a) Friedle, S.; Partyka, D. V.; Bennett, M. V.; Holm, R. H. *Inorg. Chim. Acta* **2006**, *359*, 1427. (b) Smith, A. E.; Schrauzer, G. N.; Mayweg, V. P.; Heinrich, W. *J. Am. Chem. Soc.* **1965**, *87*, 5798. (c) Wang, K.; McConnachie, J. M.; Stiefel, E. I. *Inorg. Chem.* **1999**, *38*, 4334.
(87) Lim, B. S.; Donahue, J.; Holm, R. H. *Inorg. Chem.* **2000**, *39*, 263.
(88) Pierpont, C. G.; Buchanan, R. M. *J. Am. Chem. Soc.* **1975**, *97*, 4912.
(89) Brown, G. F.; Stiefel, E. I. *Inorg. Chem.* **1973**, *12*, 2140.
(90) Cowie, M.; Bennett, M. J. *Inorg. Chem.* **1976**, *15*, 1584.
(91) (a) Boyde, S.; Garner, C. D.; Enemark, J. H.; Bruck, M. A. *J. Chem. Soc., Dalton Trans.* **1987**, 297. (b) Cervilla, A.; Llopis, E.; Marco, D.; Pérez, F. *Inorg. Chem.* **2001**, *40*, 6525. (c) Sellmann, D.; Zapf, L. *Z. Naturforsch., B Chem. Sci.* **1985**, *40b*, 380.
(92) Schulze Isfort, C.; Pape, T.; Hahn, F. E. *Eur. J. Inorg. Chem.* **2005**, 2607.
(93) Boyde, S.; Garner, C. D.; Enemark, J. H.; Bruck, M. A.; Kristofzski, J. G. *J. Chem. Soc., Dalton Trans.* **1987**, 2267.
(94) Sugimoto, H.; Furukawa, Y.; Tarumizu, M.; Miyake, H.; Tanaka, K.; Tsukube, H. *Eur. J. Inorg. Chem.* **2005**, 3088.
(95) (a) Eisenberg, R.; Ibers, J. A. *J. Am. Chem. Soc.* **1965**, *87*, 3776. (b) Eisenberg, R.; Ibers, J. A. *Inorg. Chem.* **1966**, *5*, 411. (c) Eisenberg, R.; Brennessel, W. W. *Acta Crystallogr.* **2006**, *C62*, m464.
(96) deLearie, L. A.; Haltiwanger, C.; Pierpont, C. G. *Inorg. Chem.* **1987**, *26*, 817.
(97) (a) deLearie, L. A.; Pierpont, C. G. *J. Am. Chem. Soc.* **1986**, *108*, 6393. (b) Gerber, T. I. A.; Luzipo, D.; Mayer, P. *J. Coord. Chem.* **2004**, *57*, 893.
(98) Sproules, S.; Weyhermüller, T.; Wieghardt, K., unpublished results.
(99) Griffith, W. P.; Pumphrey, C. A.; Rainey, T.-A. *J. Chem. Soc., Dalton Trans.* **1986**, 1125.
(100) Cass, M. E.; Pierpont, C. G. *Inorg. Chem.* **1986**, *25*, 122.
(101) Cass, M. E.; Green, D. L.; Buchanan, R. M.; Pierpont, C. G. *J. Am. Chem. Soc.* **1983**, *105*, 2680.
(102) (a) Frank, P.; Hodgson, K. O. *Inorg. Chem.* **2000**, *39*, 6018. (b) Frank, P.; Robinson, W. E.; Kustin, K.; Hodgson, K. O. *J. Inorg. Biochem.* **2001**, *86*, 635.

over the three ligands in a $2a_2'$ orbital whereas in the latter it is localized at the central metal ion ($3a_1'$). This difference is most clearly discerned in the ^{185,187}Re isotropic hyperfine coupling constants of both complexes which is 21 G for the former but 474 G for the latter.[95] The corresponding monocation has been assigned an electronic structure as either $[Re^{VII}(L^D)_3]^{1+}$ ($S=0$) containing a Re(VII) ion (d^0) and three closed shell catecholate(2−) ligands, or $[Re^{VI}(L^{D\bullet})(L^D)_2]^{1+}$ containing a Re(VI) ion (d^1) and a $(L_3)^{5-\bullet}$ ligand set.[95] Its structure is not known. In contrast, the trigonal prismatic monocation $[Re^V(L^{B\bullet})_2(L^B)]^{1+}$ is calculated with a central Re(V) ion (d^2; $S = 0$) and a diamagnetic ligand set $(L_3)^{4-}$ where the $2a_2'$ ligand orbital is empty (two delocalized, ligand-centered oxidative holes).

Finally, the two series $[Mo(L^A)_3]^z$ (z = 0, 1−, 2−) and $[Mo(L^B)_3]^z$ (z = 0, 1−, 2−) have been investigated.[28,32] The diamagnetic dianions $[Mo^{IV}(L^A)_3]^{2-}$ and $[Mo^{IV}(L^B)_3]^{2-}$ contain a central molybdenum(IV) ion (d^2; $S = 0$) and three dithiolate(2−) ligands, $(L^A)^{2-}$ and $(L^B)^{2-}$, respectively; the former is trigonal prismatic[66] whereas the latter is distorted trigonal prismatic ($\Theta = 24.8°$).[92] The doublet monoanions $[Mo^{IV}(L^{A\bullet})(L^A)_2]^{1-}$ and $[Mo^V(L^B)_3]^{1-}$ possess differing electronic structures. S K-edge XAS spectra clearly show that the former possesses a $(L_3)^{5-\bullet}$ ligand set with a $(2a_2')^1$ ligand orbital whereas the latter has a filled $(2a_2')^2$ orbital indicating the presence of three closed shell benzene-1,2-dithiolate(2−) ligands and a central Mo(V) ion (d^1). The following electronic structures for the $S = 0$ neutral trigonal prismatic complexes have been proposed $[Mo^V(L^{A,B\bullet})(L^{A,B})_2]^0$ and $[Mo^{IV}(L^{A,B\bullet})_2(L^{A,B})]$, for both.[28,32] Tris(dioxolene)molybdenum complexes are extremely rare. In fact, only [Mo(DBCat)$_3$] ($S = 0$) has been described.[100] Its exact electronic structure is not known.

In this work we have established that the $[V(L^{A,B})_3]^z$ series (z = 1+, 0, 1−, 2−, 3−, 4−) involves a distorted octahedral $[V^{IV}(L^{A,B})_3]^{2-}$ ($S = {}^1/_2$) Werner-type complex consisting of a central V(IV) ion ($3d^1$) with a $(3a_1')^1$ ground state and three closed-shell dianions $(L^A)^{2-}$ or $(L^B)^{2-}$, $(L_3)^{6-}$. Single electron reductions to the tri- and tetraanions are metal-centered processes producing octahedral $[V^{III}(L^{A,B})_3]^{3-}$ ($S = 1$) with a central V(III) ion ($3d^2$; $S_V = 1$) and $[V^{II}(L^{A,B})_3]^{4-}$ ($S = {}^3/_2$) with a central V(II) ion ($3d^3$; $S_V = {}^3/_2$) and three closed-shell dithiolate(2−) ligands, $(L_3)^{6-}$, respectively.

The trigonal prismatic, diamagnetic monoanions $[V^{IV}(L^{A,B\bullet})(L^{A,B})_2]^{1-}$ ($S = 0$) are singlet diradicals where a metal-centered unpaired electron at the central V(IV) ion is intramolecularly antiferromagnetically coupled to an $(L_3)^{5-\bullet}$ radical ligand set (the purely ligand-centered $2a_2'$ orbital is half-filled). The spin unrestricted Kohn−Sham calculation shows that $[V^V(L^{A,B})_3]^{1-}$ containing a V(V) ion (d^0) and three closed-shell dianionic ligands is significantly less stable and can, therefore, not represent the ground state electronic structure of these tris(dithiolene)vanadium monoanions. The paramagnetic, trigonal prismatic, neutral complexes $[V^{IV}(L^{A,B\bullet})_2(L^{A,B})]^0$ ($S = {}^1/_2$) consist of a diamagnetic $(L_3)^{4-}$ ligand set (with an empty $2a_2'$ ligand orbital). Thus, the oxidative holes are distributed over three ligands and the central vanadium ion possesses a +IV oxidation state (d^1); the complex possesses a ($3a_1'$) ground state (as does the corresponding dianion), as exemplified by their identical isotropic EPR spectra (Figure 1) and V K-pre-edge energies (Table 7).

One-electron oxidation of these neutral species yields the putative monocations $[V(L^{A,B})_3]^{1+}$. No structural or spectroscopic data is as yet available of such a species but computations (DFT) show that its electronic structure is best described as $[V^V(L^{A,B\bullet})_2(L^{A,B})]^{1+}$ ($S = 0$) where the metal-centered ($3a_1'$) d_{z^2} orbital is empty as in V(V); a diamagnetic $(L^{A,B}{}_3)^{4-}$ ligand set indicates the presence of two ligand-based oxidative holes. This molecular structure of the monocation is predicted to be distorted octahedral, $\Theta_{calcd} = 32.1°$.

The tris(dioxolene)vanadium series $[V(L^D)_3]^z$ (z = 0, 1−, 2−, 3−), where $(L^D)^{2-}$ represents an unsubstituted catecholate(2−), a 3,5-di-*tert*-butylcatecholate(2−), a tetrachlorocatecholate(2−), or an amide-containing macrocyclic catecholates,[77−83,100,101] having been thoroughly studied by X-ray crystallography and V K-edge XAS (for the mono-, di-, and trianions),[82,102] provides a truly wonderful contrast to the analogous tris(dithiolene) series. It has been clearly established that the electronic structure of the *diamagnetic octahedral* monoanion is best described as $[V^V(L^D)_3]^{1-}$ since it exhibits the highest energy V pre-edge peak at 5469.5 eV of the series. Thus, a central diamagnetic V(V) ion (d^0) is present with three closed-shell *O,O′*-coordinated catecholate(2−) ligands. Note that the corresponding dithiolene analogue is trigonal prismatic; it possesses a different electronic structure: $[V^{IV}(L^{A,B\bullet})(L^{A,B})_2]^{1-}$. The tris(dioxolene)vanadium dianion is best described as $[V^{IV}(L^D)_3]^{2-}$ ($S = {}^1/_2$). Its V pre-edge energy is observed at 5468.2 eV which is 1.3 eV lower in energy than in the monoanion.[82] This shift is strong evidence that the one-electron reduction of the monoanion is metal-centered generating a central V(IV) ion (d^1). These complexes exhibit an eight line X-band EPR spectrum with g_{iso} = 1.947−1.966, and A_{iso} = 74.6−75.2 × 10^{-4} cm^{-1} in agreement with this notion.[79,82] These parameters are similar to those for $Na_2(Et_2O)_2$-$[V^{IV}(L^E)_3]$, where $(L^E)^{2-}$ is a bulky diaryl-1,2-diketone, bis(2,6-diisopropylphenyl)gyloxal; the dioxolene equivalent to $(pdt)^{2-}$ (Scheme 3).[75] With the notable exception of the latter and $[V(BCT)]^{2-}$ (BCT = bicapped TRENCAM),[81] VO_6 compounds of this nature are (distorted) octahedral.[79,80,82] The same molecular (octahedral) and electronic structure has been observed for the dianionic tris(dithiolene)vanadium analogue. Its EPR spectrum is very similar (see Table 3), though the magnitude of the hyperfine is smaller because of the increased covalency of S-donors compared to harder O-donor ligands. Further one-electron reduction to the trianion $[V^{III}(L^D)_3]^{3-}$ ($S = 1$) is again a metal-centered process generating a central V(III) ion (d^2; $S_V = 1$), as shown by the V pre-edge energy at 5467.2 eV that is ∼0.6 eV lower in energy than is observed for the dianion.[82,102] Its structure is again octahedral.[79,83] The same holds for the dithiolene complexes $[V^{III}(L^{A,B})_3]^{3-}$ ($S = 1$).

Only very recently has a crystal structure of a neutral tris(dioxolene)vanadium complex been reported.[77] From the structure, the complex was formulated as $[V^V(3,6\text{-DBSQ}^\bullet)$-$(3,6\text{-DBCat})_2]^0$ ($S = {}^1/_2$), comprising two *O,O′*-coordinated 3,6-di-*tert*-butylcatecholate(2−) ligands and one localized *O,O′*-bound 3,6-di-*tert*-butylbenzenesemiquinonate(1−) π radical. Consequently, the central vanadium ion possesses a +V (d^0) oxidation state. The VO_6 polyhedron is *octahedral*. The X-band EPR spectrum is centered about a g_{iso} value of 2.0058, and a small $A(^{51}V)$ superhyperfine coupling of 3.47 G has been reported. Moreover, the spectrum exhibits additional features attributed to a $A(^1H)$ hyperfine interaction of 4.53 G. These data unambiguously indicate the presence of a ligand π radical coupled to a diamagnetic vanadium(V) center. A careful analysis of the C−C and C−O bond distances

suggested to the authors that "some semiquinone character for the catecholate ligands could result from either crystallographic disorder or a shift in the charge distribution to, conceivably, a $[V^{III}(3,6\text{-}DBSQ^{\bullet})_3]$ redox isomer". V K-edge XAS measurements on this compound enable one to distinguish between the a V(V) and V(III) ion. Our BS(3,2) DFT calculations using the B3LYP functional on this complex clearly point to a $[V^{III}(3,6\text{-}DBSQ^{\bullet})_3]$ electronic structure (Supporting Information, Figure S41), where the two unpaired electrons at the central vanadium ion are coupled antiferromagnetically to two semiquinonate(1−) radicals (Supporting Information, Scheme S16); the residual unpaired electron would then reside on the third semiquinonate radical in agreement with the reported EPR spectrum. The proposed V(V) solution did not arise in any of the calculations of this compound. Interestingly, the corresponding neutral, *trigonal prismatic* tris(dithiolene)vanadium complexes possess a distinctly different electronic structure, namely, $[V^{IV}(L_3{}^{4-})]^0$ containing a central V(IV) ion (d^1) and a diamagnetic ligand set $(L_3)^{4-}$. Their EPR spectra display parameters: $g \sim 1.985$ and $A(^{51}V) \sim 58 \times 10^{-4}\ cm^{-1}$ (~64 G) typical for a vanadium(IV) ion with an unpaired electron in the metal-centered $3a_1'$ orbital, $(d_{z^2})^1$.

Perhaps the most engaging computational result is displayed in Figure 9. Previously, we had investigated the total energy of a simple neutral tris(dithiolene)vanadium complex as a function of the twist angle, and seen that the trigonal prismatic structure is significantly more stable than the octahedral one (~17 kcal mol^{-1}). The plot for the neutral vanadium tris(catecholate) complex as a function of the twist angle produces the opposite result. Here, the most stable geometry is the octahedral structure, with $\Theta_{calcd} = 49.2°$ being the same magnitude as the angle derived from optimization, and near to the crystallographic value of 46.7°. At $\Theta < 12°$, there is a small jump to another potential energy surface that although abrupt is physically meaningful. Here, for the tris(catecholate) complex, the electronic structure is defined as $[V^{IV}(L_3{}^{4-})]^0$, which is 10 kcal mol^{-1} more unstable than the octahedral geometry. It should be noted that several hundred SCF iterations were required to converge these unrealistic trigonal prismatic geometries. This plot does show the difference in bonding between dioxolene and dithiolene ligands, in that the energy separation between the S 3p and M d orbitals is significantly less than the corresponding energy difference with the O 2p orbitals. These highly covalent V−S π bonds contribute to an almost 20% reduction in the ^{51}V hyperfine interaction when comparing analogous dianionic complexes.

Conclusions

The six-membered vanadium tris(dithiolene) electron transfer series has been probed by X-ray absorption spectroscopy that neatly augments other spectroscopic data collected over many years of investigating this system. The neutral, monoanionic, and dianionic members are connected via ligand-centered redox processes that involves varying the occupancy of the purely ligand $2a_2'$ MO. These vanadium compounds follow the general trends for discerning trigonal prismatic versus octahedral coordination.[89] Population of the $2a_2'$, and more profoundly, the $5e'$ state, which are both antibonding with respect to a trigonal prism, sees the geometries twist toward a more preferred octahedral conformation for the dianion, trianion, and tetraanion. Interestingly, the diamagnetic monoanion is a singlet diradical, and the folding of the dithiolene ligands that reduces the symmetry to C_{3h}, appears to facilitate strong antiferromagnetic coupling between the $3a_1'$ and $2a_2'$ magnetic orbitals. Notably, the isoelectronic neutral molybdenum species all crystallize with a similar degree of ligand folding,[28,34,86,87,90] whereas the monocationic rhenium compound is calculated with perfectly flat dithiolene ligands.[34]

The strength of the predominately V−S π bonding $4e'$ appears to be the adhesive that maintains the trigonal prismatic VS_6 array. With very little metal character, these orbitals could almost be described as the sulfur−sulfur bond that was favored by previous forays into understanding the origins of trigonal prismatic coordination,[5,6,16,89,90,103] in that the dimensions of the prism were virtually constant despite the stark changes in the ionic radius of the metal. However, there were examples that refuted this hypothesis,[104] and so it was difficult to clarify the underlying electronic factors that generate this geometry. Furthermore, there are examples of the same tris(dithiolene) complex anion with different trigonal twist angles when crystallized with different countercations,[94,105] though this is only noted for second- and third-row transition metals; this vanadium tris(dithiolene) series does not exhibit the same structural anomalies. Moreover, as a first-row metal, vanadium has a long core-hole lifetime that facilitates a well-separated pre-edge and rising edge such that we could conveniently determine the complex geometry for solids as well as solution samples.

This spectroscopic and computational study has provided a clear picture of the electronic structures of the tris(dithiolene)vanadium transfer series that ultimately provides a solid foundation on which to begin understanding the origins of the trigonal prismatic geometry that is so pervasive in tris(dithiolene) coordination chemistry.

Acknowledgment. We are especially grateful to the rigorous and thorough examination of this manuscript by one reviewer. We are grateful for financial support from the Fonds der Chemischen Industrie. S.S. thanks the Max-Planck-Society for a postdoctoral fellowship. SSRL operations are funded by the Department of Energy, Office of Basic Energy Sciences. The Structural Molecular Biology program is supported by the National Institutes of Health (Grant 5 P41 RR001209), National Center for Research Resources, Biomedical Technology Program and by the Department of Energy, Office of Biological Environmental Research.

Supporting Information Available: X-ray crystallographic files in CIF format for **1a**, **1b**, **2c**, and **3b**. Fluid and frozen solution EPR spectra for all neutral and dianionic species; magnetic susceptibility data for **6**; cyclic voltammograms for **3c**, **4c**, and **5a**; electronic absorption spectra of $[V(bdt)_3]^z$ ($z = 1-$, $2-$, $3-$), $[V(tdt)_3]^z$ ($z = 1-$, $2-$, $3-$), and $[V(edt)_3]^z$ ($z = 0$, $1-$, $2-$); experimental and calculated V K-edge spectra of **2b** and **4c**, and S K-edge spectra of **2c**, **3c**, **4c**, and **6**; and pseudo Voigt deconvolution of the S K-edge spectra of **2c**, **3c**, **4c**, and **6**. Tables of geometric and electronic structures details (qualitative MO schemes and Mulliken spin density plots) of all calculated structures. This material is available free of charge via the Internet at http://pubs.acs.org.

(103) (a) Eisenberg, R. *Prog. Inorg. Chem.* **1970**, *12*, 295. (b) Stiefel, E. I.; Eisenberg, R.; Rosenberg, R. C.; Gray, H. B. *J. Am. Chem. Soc.* **1966**, *88*, 2956.
(104) Cowie, M.; Bennett, M. J. *Inorg. Chem.* **1976**, *15*, 1589.
(105) Beswick, C. L.; Schulman, J. M.; Stiefel, E. I. *Prog. Inorg. Chem.* **2004**, *52*, 55.